Transport in curved nanoribbons in a magnetic field

B. Novakovic,[1,*] R. Akis,[2] and I. Knezevic[1,†]

[1]*Department of Electrical and Computer Engineering, University of Wisconsin—Madison, Madison, Wisconsin 53706, USA*

[2]*Department of Electrical Engineering, Fulton School of Engineering, Arizona State University, Tempe, Arizona 85287, USA*

(Received 4 August 2011; revised manuscript received 5 October 2011; published 4 November 2011)

We study the low-field and ballistic electronic transport in curved nanoribbons subject to static and uniform magnetic fields, where the curved nanoribbon is placed between two leads that inject scattering states. The method we present is based on a tight-binding form of the time-independent two-dimensional Schrödinger equation in curvilinear coordinates, with electric scalar and magnetic vector potentials included, and it enables a numerical description of transport in arbitrarily shaped curved nanostructures. A description of transport in terms of the scattering-state basis in the presence of magnetic field, together with curvature and possibly misaligned contacts, requires the use of a local Landau gauge. Based on the use of a stabilized transfer matrix method, we compute the conductance and normalized electronic density at the Fermi level for several curved nanoribbons in cylindrical and toroidal geometry, with and without the magnetic field. The magnetic field determines the number of injected propagating modes by affecting the Landau-level energies in the contacts, while a complex interplay between the magnetic field and the nanoribbon shape (both its curvature and helicity) determines the transmission of injected modes.

DOI: 10.1103/PhysRevB.84.195419 PACS number(s): 73.63.−b, 73.23.Ad, 73.50.−h, 05.60.Gg

I. INTRODUCTION

Curved nanoribbons are narrow nonplanar strips fashioned from semiconductor heterostructures that support a two-dimensional (2D) electron gas.[1,2] They are among a growing variety of curved nanostructures that can be fabricated today.[3–6] Curved nanostructures can be produced from planar heterostructures by selective underetching in combination with strain mismatch.[3,7–10] Other methods involve transfer from planar to curved substrates,[11] growth of curved layers using curved templates (nanowires, nanotubes, or nanorings) as substrates,[12–15] or thermal transformation of curved templates.[16] Among the most prominent curved structures are flexible electronic devices,[17,18] used for applications ranging from flexible integrated circuits[19] to artificial retinas.[20] Techniques such as dry transfer printing[19,21] and electrohydrodynamic jet printing[22] have been developed to enable deposition of electronic devices onto flexible substrates, such as polymers.[2,23]

Curvature presents a novel, mechanical degree of freedom available for tailoring these nanostructures' physical properties. Theoretical and experimental investigations of optical properties of curved nanostructures for various resonators,[24–29] photoluminescence tuning,[30,31] coherent emission and lasing,[32,33] and metamaterials[34] have been reported. There have also been a number of papers on magnetic properties of curved nanostructures: magnetization,[35–38] spin-orbit interaction,[39,40] and spin-wave confinement and interference.[41,42]

Theoretical work on the electronic properties of curved nanostructures has so far been largely focused on the effects of the curvature-induced geometric potential and the classification of states,[43–49] as well as transport[50–53] in simple structures with analytical shapes (e.g., cylindrical or with periodic corrugation). Similar features have been addressed experimentally.[54–58] Considering that experimentally fabricated nanostructures typically have imperfections in shape,[3] there is a need for a theoretical approach, necessarily computationally based, that is capable of addressing transport in arbitrarily shaped curved nanostructures.

Within the envelope function and effective mass framework, electronic states in curved nanostructures can be obtained by solving the 2D Schrödinger equation (SE) in curvilinear coordinates, derived from the three-dimensional (3D) SE in the limit of zero thickness.[59–62] The problem of including arbitrary magnetic fields into the 2D SE through the covariant Peierls substitution has been solved recently.[63] It has been shown that the dynamics of a particle on the surface can be decoupled from the one along the normal to the surface by using a suitable gauge transformation in the derivation of the 2D SE. In the same work, analytic forms of the 2D SE with magnetic field have been given for spherical, cylindrical, and toroidal coordinate systems. As the low-field and nearly ballistic quantum transport in nanostructures at low temperatures is dictated by the transmission properties of the states in the vicinity of the Fermi level,[64–67] a theoretical account of electronic transport in curved nanostructures in this regime can, therefore, be described by solving the 2D SE in curvilinear coordinates with open boundary conditions.

In this paper, we study the linear and ballistic transport properties, specifically the electronic density and conductance, of curved nanoribbons subject to a static magnetic field. The presented theoretical and numerical framework is based on a tight-binding form of the time-independent two-dimensional Schrödinger equation in curvilinear coordinates and is entirely general: it enables a computational description of ballistic transport in an arbitrarily shaped two-terminal curved nanostructure. A curved nanostructure is connected to large reservoirs via leads that are the source/drain for scattering states. We adopt a suitable orthogonal curvilinear coordinate system to parametrize a generic curved surface and discretize the 2D SE, due to Ferrari and Cuoghi,[63] by using a second-order finite-difference scheme. We explain the Hermiticity properties of the discretized curvilinear Hamiltonian and discuss the local Landau gauge used to include arbitrarily directed

magnetic fields in the leads and in the curved nanoribbons. We also compare the Peierls phase approximation with the exact way of including the magnetic field in the curvilinear 2D SE. The obtained tight-binding form of the 2D SE in curvilinear coordinates can be solved by well-established numerical methods for planar nanostructures, such as the transfer matrix,[68–70] scattering matrix,[71,72] recursive Green's function,[73] and nonequilibrium Green's function techniques.[67] We use the stabilized transfer matrix approach due to Usuki *et al.*,[68] since it provides both the transmission/reflection coefficients and a convenient way to reconstruct the wave function. By using the Landauer formula[67] to calculate the conductance from the transmission coefficients, as well as by using the wave function to calculate the electron density, we show that coherent electron transport is affected by the curvature and magnetic field through the number of injected propagating modes (modulated by the magnetic field flux in the leads) and their transmission properties (determined by the interplay between the magnetic field and the nanoribbon's curvature and helicity).

This paper is organized as follows. In Sec. II, we lay out the theoretical concepts and the corresponding numerical model. We explain how the surface divergence, which appears in the curvilinear 2D SE, is related to the curvature properties and the normal component of the magnetic vector potential. In Sec. II A, we start from the 2D SE in curvilinear coordinates, with the electric scalar potential and the magnetic vector potential included, and focus on the curvilinear Laplacian by explaining its Hermitian properties and how they are affected by its finite-difference version. We present several discretization schemes that may be used. In Sec. II B, we derive a tight-binding form of the 2D SE in curvilinear coordinates by using a second-order finite-difference scheme. We analyze the consequences of the non-Hermitian nature of the tight-binding (discretized) curvilinear Hamiltonian matrix. In Sec. II C, we explore the conditions for the validity of the Peierls phase approximation. In Sec. II D, we explain how the magnetic field is included in the lead/curved nanoribbon/lead system. We discuss the necessity of using the Landau gauge in the leads to ensure proper mode injection and discuss cases in which a local Landau gauge (amounting to a continuous gauge transformation) may need to be applied to the curved nanoribbon. In Sec. III, we apply the described numerical technique to calculate the electron density at the Fermi level and conductance in several nanoribbons in cylindrical and toroidal geometries, with and without the magnetic field. A summary and concluding remarks are given in Sec. IV.

II. THEORETICAL AND NUMERICAL FRAMEWORK

Conductance in the linear, ballistic, steady-state quantum transport regime in nanoribbons is determined by the transmission properties of the electronic states near the Fermi level.[65–67] In curved nanoribbons, we will calculate the transmission and electron density near the Fermi level from the time-independent 2D SE in curvilinear coordinates in the scattering-state basis. As shown previously, by starting from the 3D SE and using the covariant Peierls substitution and a layer thinning procedure,[63] one can arrive at its 2D version completely decoupled from the direction normal to the thin curved surface. We state this equation in its time-independent form

$$\frac{1}{2m}\big[-\hbar^2\nabla_S^2\psi + ie\hbar\nabla_S\cdot\vec{A}_S\psi + 2ie\hbar g^{ij}A_i\partial_j\psi + e^2g^{ij}A_iA_j\psi\big] + V\psi = E\psi, \quad (1)$$

where the 2D curvilinear Laplacian is given by

$$\nabla_S^2\psi = \frac{1}{\sqrt{g}}\partial_i(\sqrt{g}g^{ij}\partial_j\psi) \quad (2)$$

and the 2D curvilinear divergence by

$$\nabla_S\cdot\vec{A}_S = \frac{1}{\sqrt{g}}\partial_i(\sqrt{g}g^{ij}A_j). \quad (3)$$

Here, $\partial_i \equiv \partial/\partial u^i$, $\vec{A}_S = (A_1, A_2, 0)$, u^i is a curvilinear coordinate on the surface S (here only $i = 1,2$ are included since the normal component $i = 3$ has been decoupled), A_i are the covariant components of the magnetic vector potential, g^{ij} are the contravariant components of the metric tensor, g is the determinant of the metric tensor with covariant components, $V = e\Phi + V_s$, Φ is the electric scalar potential, and V_s is the geometric potential given by

$$V_s = -\frac{\hbar^2}{8m}[k_1 - k_2]^2, \quad (4)$$

where k_1 and k_2 are the principal curvatures of the surface S.[74]

It can be shown (see Appendix A) that there is a connection between the surface divergence $\nabla_S\cdot\vec{A}_S$, the curvature properties, and the normal component of the vector potential A_3. Assuming an orthogonal coordinate system and $\nabla\cdot\vec{A} = 0$, the following relation holds

$$\nabla_S\cdot\vec{A}_S = \frac{1}{g}A_3|_{u^3=0}(g_{11}h_{22} + g_{22}h_{11}) - \left.\frac{\partial A_3}{\partial u^3}\right|_{u^3=0}, \quad (5)$$

where h_{ij} are the elements of the second fundamental form of the surface (covariant components of the metric tensor, g_{ij}, being the elements of the first fundamental form of the surface)[74] and A_3 is the projection of $\vec{A}$ onto the normal to the curved surface (it simply corresponds to the component of $\vec{A}$ along the normal to the surface). We can further introduce effective potentials due to the magnetic vector potential

$$V_3 = \frac{1}{2m}e\hbar\nabla_S\cdot\vec{A}_S\,, \quad (6a)$$

$$V_S = \frac{1}{2m}e^2g^{ij}A_iA_j\,, \quad (6b)$$

where V_3 and V_S define the potentials due to the normal component A_3 and the surface component $\vec{A}_S$, respectively. We can now rewrite Eq. (1) in the form

$$\frac{1}{2m}\big[-\hbar^2\nabla_S^2\psi + 2ie\hbar g^{ij}A_i\partial_j\psi\big] + V_{\rm eff}\psi = E\psi, \quad (7)$$

where $V_{\rm eff} = V + V_S + iV_3$. Let us further rescale the previous equation, for convenience that will become apparent shortly, by multiplying it by $\sqrt{g}$. We get

$$\frac{1}{2m}\big[-\hbar^2\overline{\nabla}_S^2\psi + 2ie\hbar\sqrt{g}g^{ij}A_i\partial_j\psi\big] + \sqrt{g}V_{\rm eff}\psi = \sqrt{g}E\psi, \quad (8)$$

where $\overline{\nabla}_S^2 = \partial_i(\sqrt{g}g^{ij}\partial_j) \equiv \sqrt{g}\nabla_S^2$. At the end, it should be mentioned that the Hamiltonian, as given by Eq. (1), is Hermitian (see Appendix B 1).

A. Curvilinear Laplacian in the tight-binding form

Unlike its Cartesian counterpart, the curvilinear Laplacian given by Eq. (2) can only be Hermitian up to the prefactor $1/\sqrt{g}$ once it is cast into a finite-difference form.[75,76] In other words, it is Hermitian only up to a truncation error of the Taylor expansion by which a particular finite-difference scheme is derived. A finite-difference approximation of the planar Hamiltonian gives a Hermitian Hamiltonian matrix, as is well known, while the same approximation of the curvilinear Hamiltonian in the curved nanoribbon can yield a non-Hermitian Hamiltonian matrix. The latter will be derived in more detail in this section and in Sec. II B. By rescaling the Laplacian, as in Eq. (8), we remove this Hermiticity problem from the rescaled Laplacian, and, consequently, from the rescaled Hamiltonian, by moving the prefactor that prevents achieving the Hermiticity to the main diagonal. The problem of finding appropriate discretization schemes for the rescaled Hamiltonian in Eq. (8) is easier than for the original Hamiltonian from Eq. (7). The non-Hermiticity can be minimized by choosing a sufficiently small grid size, such that $\sqrt{g}$ does not vary too much across one grid cell. In the limit where curvature is constant (like in a cylinder), the curvilinear tight-binding Hamiltonian, obtained using the finite differences, is exactly Hermitian. Sufficiently smooth curvature variation on the finite-difference grid is also important to be able to capture potentially sharp curvature features.

In order to determine which conditions should be met to have a small variation of $\sqrt{g}$ over one grid cell, we can imagine an orthogonal coordinate system and refer to the definition of the metric tensor ($g_{ii} = \partial\vec{r}/\partial u^i \partial\vec{r}/\partial u^i$), which is diagonal in that case. If we assume that the curvilinear coordinate u^i is angular, the metric tensor component g_{ii} at any point will be equal to the squared radius of the curvature at that point along u^i. First, we need enough points on the surface to capture all the curvature features. Therefore, the grid size (in radians) should satisfy $\Delta u^i \ll 1$, meaning that the radius of the curvature should be much larger than the grid size (in meters) along the geodesic in that point. So, a grid size of 1 nm will generate a fine-enough mesh for curvature radii not smaller then a few tens of nanometers. Second, the radii of curvature in both surface directions should vary smoothly and slowly over neighboring points; in other words, the relative change in the grid size along the geodesic should be much smaller than 1. The second requirement can be visualized by first defining a uniform (constant grid size) rectangular grid on a planar surface and then introducing curvature, due to which the grid will become nonuniform [Fig. 1(b)]. We can then assess the metric tensor variations by knowing the relative change in the grid size along the geodesic over neighboring points.

Even after the rescaling, Eq. (8), we still cannot use arbitrary finite-difference schemes, but only those that preserve the Hermiticity of the rescaled Laplacian $\overline{\nabla}_S^2$. The reason for possible non-Hermiticity in arbitrary finite-difference schemes are the off-diagonal terms of the metric tensor ($g^{12} = g^{21}$ or $g_{12} = g_{21}$), which are nonzero if the coordinate system is not orthogonal. Among possible finite-difference schemes to discretize $\overline{\nabla}_S^2$, we will mention two: The four-point formula (Fig. 1) given by

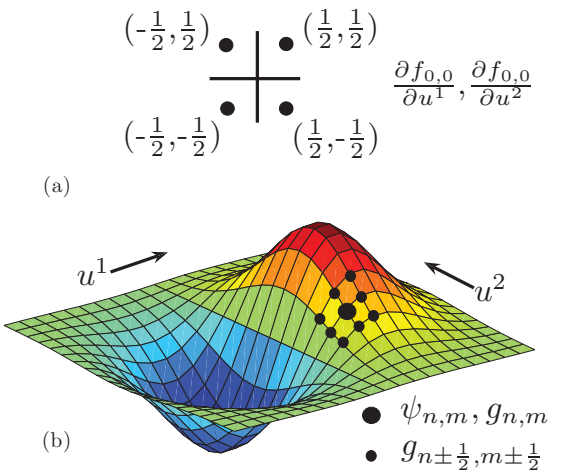

FIG. 1. (Color online) (a) The four-point scheme for discretization of the first partial derivatives by using Eq. (9). (b) An example of a curved surface parametrized by curvilinear coordinates u^1 and u^2. Leads are planar continuations of the curved surface in both directions along the longitudinal coordinate u^1. In order to calculate the wave function value at the grid point denoted by the large solid circle (central point) from the four-point scheme, we have to know the metric tensor values at all the surrounding points, denoted by the small solid circles, as well as at the central point.

$$\begin{aligned}\frac{\partial f_{0,0}}{\partial u^1} &= \frac{1}{2\Delta_1}\left(f_{\frac{1}{2},\frac{1}{2}} - f_{-\frac{1}{2},\frac{1}{2}} + f_{\frac{1}{2},-\frac{1}{2}} - f_{-\frac{1}{2},-\frac{1}{2}}\right) + \mathcal{O}\left(\Delta_1^2\right),\\ \frac{\partial f_{0,0}}{\partial u^2} &= \frac{1}{2\Delta_2}\left(f_{\frac{1}{2},\frac{1}{2}} + f_{-\frac{1}{2},\frac{1}{2}} - f_{\frac{1}{2},-\frac{1}{2}} - f_{-\frac{1}{2},-\frac{1}{2}}\right) + \mathcal{O}\left(\Delta_2^2\right),\end{aligned} \tag{9}$$

where Δ_1 and Δ_2 are the grid sizes along u^1 and u^2 axes, respectively, and the central difference scheme (by simultaneously using two different grid sizes)[75]

$$\frac{\partial f_{0,0}}{\partial u^{1(2)}} = \begin{cases} \frac{f_{\frac{1}{2},0\left(0,\frac{1}{2}\right)} - f_{-\frac{1}{2},0\left(0,-\frac{1}{2}\right)}}{\Delta_{1(2)}}, & i = j \quad \text{in} \quad \overline{\nabla}_S^2 \\ \frac{f_{1,0(0,1)} - f_{-1,0(0,-1)}}{2\Delta_{1(2)}}, & i \neq j \quad \text{in} \quad \overline{\nabla}_S^2 \end{cases}. \tag{10}$$

Here, we will work only with orthogonal coordinate systems, in which case there is no need for the more complicated finite-difference schemes given by Eqs. (9) and (10) and the ordinary central-difference scheme is enough. [Actually, in the limit $g^{ij} = g_{ij} = 0, i \neq j$, the term in Eq. (10) for which $i \neq j$ vanishes from $\overline{\nabla}_S^2$ and we are left with the ordinary central-difference scheme]. In the case a nonorthogonal coordinate system is needed, we can go back and use (9) or (10) and follow the procedure outlined in the rest of this section. So, considering an orthogonal coordinate system and applying the ordinary central-difference scheme we can come up with a

tight-binding representation of $\overline{\nabla}_S^2$, discretized at some slice n, as

$$-\frac{\hbar^2}{2m}\left(\overline{\nabla}_S^2\psi\right)_n = \mathbf{L}_n\boldsymbol{\Psi}_n + \mathbf{L}_{n,n-1}\boldsymbol{\Psi}_{n-1} + \mathbf{L}_{n,n+1}\boldsymbol{\Psi}_{n+1}, \tag{11}$$

where $\boldsymbol{\Psi}_n$ is a column vector containing all wave function values on the nth slice (slice is a set of all points with the longitudinal coordinate u^1 constant) and the $(M+1)\times(M+1)$ matrices $\mathbf{L}$ are given by

$$\mathbf{L}_n = \begin{bmatrix} c_{n,0} & -f_2^0 e_{n,0}^{+\frac{1}{2}} & 0 & \cdots & 0 \\ -f_2^1 e_{n,1}^{-\frac{1}{2}} & c_{n,1} & -f_2^1 e_{n,1}^{+\frac{1}{2}} & \cdots & 0 \\ 0 & -f_2^2 e_{n,2}^{-\frac{1}{2}} & c_{n,2} & \cdots & 0 \\ \vdots & \vdots & \vdots & \vdots & \vdots \\ 0 & \cdots & 0 & -f_2^M e_{n,M}^{-\frac{1}{2}} & c_{n,M} \end{bmatrix}, \tag{12a}$$

$$\mathbf{L}_{n,n\pm1} = \begin{bmatrix} -f_1^n d_{n,0}^{\pm\frac{1}{2}} & 0 & \cdots & 0 \\ 0 & -f_1^n d_{n,1}^{\pm\frac{1}{2}} & \cdots & 0 \\ \vdots & \vdots & \vdots & \vdots \\ 0 & \cdots & 0 & -f_1^n d_{n,M}^{\pm\frac{1}{2}} \end{bmatrix}, \tag{12b}$$

where

$$\begin{aligned} c_{n,m} &= f_1^n d_{n,m}^{+\frac{1}{2}} + f_1^n d_{n,m}^{-\frac{1}{2}} + f_2^m e_{n,m}^{+\frac{1}{2}} + f_2^m e_{n,m}^{-\frac{1}{2}}, \\ d_{n,m}^l &= t_1^{n+l}(\sqrt{g}g^{11})_{n+l,m}, \\ e_{n,m}^l &= t_2^{m+l}(\sqrt{g}g^{22})_{n,m+l}, \end{aligned} \tag{13}$$

with $t_{1(2)}^{i+l} = \hbar^2/2m\Delta_{1(2)}^i$ for $0 \leqslant l < 1$, $f_{1(2)}^i = 2/(\Delta_{1(2)}^i + \Delta_{1(2)}^{i-1})$ and $M+1$ the number of points in a slice. The assumption is that M is constant for all slices. If the curved nanoribbon has varying width, we can always set a hardwall potential at the extra points around the narrow regions. We assume a 2D nonuniform curvilinear grid, with Δ_1^n the longitudinal grid size between slices n and $n+1$ and Δ_2^m the transversal grid size between points m and $m+1$ along a slice. Equation (11) reflects the lack of symmetry between the two curvilinear surface directions in our problem: There is the longitudinal direction with open boundaries, along which the current flows carried by complex traveling waves, and the transversal direction along which the potential defines the shape of real (confined) transverse modes. This form of Eq. (11) makes it suitable for use with the transfer matrix method, where the slice wave functions (containing all transverse points) are transferred along the longitudinal direction.

The form of the matrix (12a) will depend on the boundary conditions in the u^2 direction. While the system is always open in the longitudinal (i.e., transport) direction along the coordinate u^1, it might be either closed (hardwall potential) or periodic (e.g., closing onto itself, like in a cylinder) in the transverse direction u^2. In the former case we use the Dirichlet boundary conditions, which give the form (12a), while in the latter the periodic boundary conditions, where we have the following additional terms

$$\begin{aligned} \mathbf{L}_n(1,M+1) &= -f_2^0 e_{n,0}^{-\frac{1}{2}}, \\ \mathbf{L}_n(M+1,1) &= -f_2^M e_{n,M}^{+\frac{1}{2}}. \end{aligned} \tag{14}$$

If the coordinate system is not orthogonal ($g^{ij} \neq 0, i \neq j$) and we use either one of the schemes (9) or (10), then, besides having more complex matrix elements, $\mathbf{L}_{n,n\pm1}$ would also depend on the boundary condition in the transverse direction (being a three-diagonal matrix in that case).

B. The tight-binding 2D Schrödinger equation

We will now discretize the rest of Eq. (8) to obtain the curvilinear 2D SE in the tight-binding form. To avoid having imaginary potential on the main diagonal of the Hamiltonian matrix, we will first rewrite the imaginary terms containing the magnetic vector potential in Eq. (8) as

$$\begin{aligned} &2ie\hbar\sqrt{g}g^{ij}A_i\partial_j\psi + ie\hbar\sqrt{g}\nabla_S\cdot\vec{A}_S\psi \\ &\quad = ie\hbar\sqrt{g}g^{ij}A_i\partial_j\psi + ie\hbar\partial_i(\sqrt{g}g^{ij}A_j\psi). \end{aligned} \tag{15}$$

Since these terms contain the first derivative of the wave function, we will use the central-difference scheme like for the case $i \neq j$ in Eq. (10), in order to avoid having wave-function values at half-integer grid points. We obtain the following tight-binding form at some slice n

$$\begin{aligned} &\frac{ie\hbar}{2m}[\sqrt{g}g^{ij}A_i\partial_j\psi + \partial_i(\sqrt{g}g^{ij}A_j\psi)]_n \\ &\quad = \mathbf{P}_n\boldsymbol{\Psi}_n + \mathbf{P}_{n,n-1}\boldsymbol{\Psi}_{n-1} + \mathbf{P}_{n,n+1}\boldsymbol{\Psi}_{n+1}, \end{aligned} \tag{16}$$

where

$$\begin{aligned} \mathbf{P}_n(m,m+1) &= \frac{ie}{\hbar}f_2^{m-1}\frac{1}{2}\left[e_{n,m-1}^0 A_2(n,m-1)\Delta_2^{m-1}\right. \\ &\quad \left. + e_{n,m-1}^{+1}A_2(n,m)\Delta_2^m\right], \\ \mathbf{P}_n(m,m-1) &= -\frac{ie}{\hbar}f_2^{m-1}\frac{1}{2}\left[e_{n,m-1}^0 A_2(n,m-1)\Delta_2^{m-1}\right. \\ &\quad \left. + e_{n,m-1}^{-1}A_2(n,m-2)\Delta_2^{m-2}\right], \\ \mathbf{P}_{n,n\pm1}(m,m) &= \pm\frac{ie}{\hbar}f_1^n\frac{1}{2}\left[d_{n,m-1}^0 A_1(n,m-1)\Delta_1^n\right. \\ &\quad \left. + d_{n,m-1}^{\pm1}A_1(n\pm1,m-1)\Delta_1^{n\pm1}\right]. \end{aligned} \tag{17}$$

(The matrix indices in the above equations are $m \in [1,M]$, $m \in [2,M+1]$, and $m \in [1,M+1]$, respectively). Note that when m is used as a matrix index on the left-hand side of Eqs. (17) its range is $[1,M+1]$, while the corresponding transverse grid position on the right-hand side is in the range $[0,M]$, hence $m-1$ is used on the right-hand side. The magnetic vector potential components in Eqs. (17) are the covariant components, given by $\vec{A} = A_i\vec{e}^i$, where $\vec{e}^i = \nabla u^i$. The relations of the covariant components to the contravariant components $\vec{A} = A^i\vec{e}_i$, where $\vec{e}_i = \partial\vec{r}/\partial\vec{u}^i$, are $A_1 = g_{11}A^1$ and $A_2 = g_{22}A^2$, if the coordinate system is orthogonal. The relations to the magnetic vector components expressed with respect to the unit curvilinear vectors $\vec{a}_i$, $\vec{A} = \overline{A}^i\vec{a}_i$, which is often done if one starts with calculating $\vec{A}$ in the Cartesian coordinate system and then performs either a coordinate

system transformation to the desired curvilinear system or a vector projection in the case of arbitrary curvature, are $A_1 = \sqrt{g_{11}}\overline{A}^1$ and $A_2 = \sqrt{g_{22}}\overline{A}^2$. In the case of using $\overline{A}^{1(2)}$ we see that it should be multiplied by the actual grid size along the geodesic (in meters), $(\sqrt{g_{11(22)}})_{n,m}\Delta^{n(m)}_{1(2)}$, at the grid position (n,m).

As with the $\mathbf{L}$ matrices in Eqs. (12), if the transverse boundary condition is periodic, we have additional terms of the following form in Eqs. (17)

$$\begin{aligned}\mathbf{P}_n(1,M+1) &= -\frac{ie}{\hbar} f_2^0 \frac{1}{2}\left[e^0_{n,0}A_2(n,0)\Delta_2^0 \right.\\ &\quad \left. + e^{-1}_{n,0}A_2(n,M)\Delta_2^M\right],\\ \mathbf{P}_n(M+1,1) &= \frac{ie}{\hbar} f_2^M \frac{1}{2}\left[e^0_{n,M}A_2(n,M)\Delta_2^M \right.\\ &\quad \left. + e^{+1}_{n,M}A_2(n,0)\Delta_2^0\right].\end{aligned} \tag{18}$$

Finally, the tight-binding 2D SE can be written as

$$\boldsymbol{H}_{n,n+1}\boldsymbol{\Psi}_{n+1} + \boldsymbol{H}_{n,n-1}\boldsymbol{\Psi}_{n-1} + \boldsymbol{H}_n\boldsymbol{\Psi}_n = E\boldsymbol{G}_n\boldsymbol{\Psi}_n, \tag{19}$$

with

$$\boldsymbol{G}_n = \begin{bmatrix} (\sqrt{g})_{n,0} & 0 & \cdots & 0 \\ 0 & (\sqrt{g})_{n,1} & \cdots & 0 \\ \vdots & \vdots & \vdots & \vdots \\ 0 & \cdots & 0 & (\sqrt{g})_{n,M} \end{bmatrix}, \tag{20}$$

and

$$\begin{aligned}\boldsymbol{H}_n &= \mathbf{L}_n + \mathbf{P}_n + \mathbf{G}_n\boldsymbol{V}_n,\\ \boldsymbol{H}_{n,n\pm1} &= \mathbf{L}_{n,n\pm1} + \mathbf{P}_{n,n\pm1},\end{aligned} \tag{21}$$

where $\boldsymbol{V}_n$ is a column vector containing the potential $V_{\text{eff}} - iV_3 = V + V_S$ of the nth slice (since iV_3 is already incorporated into the $\boldsymbol{P}_n$ and $\boldsymbol{P}_{n,n\pm1}$ matrices).

Equation (19) is *the central equation of this paper*. Its form is similar to that of the planar case,[68,73] but with more complicated matrix elements. In order to solve it, we make use of the stabilized transfer matrix technique due to Usuki *et al.*,[68] because it provides both the reflection/transmission coefficients and a convenient way to calculate the wave functions needed for electron density calculation. The modified stabilized transfer matrix technique, as used in this work, is described in detail in Appendix C.

Although Eq. (19) is derived from the exact curvilinear Schrödinger equation [Eq. (1)], the usual discretization error, associated with the second-order finite-difference scheme, here may lead to a non-Hermitian tight-binding Hamiltonian. The non-Hermiticity stems from the discretization of the curvilinear Laplacian in the case when curvature is spatially nonuniform, as explained in Sec. II A, and/or from the fact that we allow the curvilinear grid to be nonuniform in general. The Hermiticity of a discretized Hamiltonian matrix is a desirable property, because it makes the numerical solution of the eigenvalue problem easier. Even though our computational method requires the solution of the eigenvalue problem only in the leads—which are typically, but not necessarily, flat, so the Hamiltonian in them is Hermitian—we employed discretization schemes in Eq. (19) that enable the construction of a discretized non-Hermitian curvilinear Hamiltonian whose eigenvalue problem can be mapped onto that of a Hermitian matrix with the help of certain matrix transformations. In Appendix B, we give a detailed account of the Hermitian properties of both the exact and the tight-binding Hamiltonians, along with the aforementioned matrix transformations. After transforming the original non-Hermitian eigenvalue problem, we obtain a Hermitian eigenvalue problem with the same eigenvalues and transformed wave functions. From this we draw two conclusions: First, the eigenvalue problem becomes more manageable computationally, albeit with the additional reverse transformation necessary to reconstruct the original wave functions, and, second, although the transformed wave functions do form a complete and orthonormal basis, being eigenvectors of a Hermitian matrix, our original wave functions may not form such a basis. However, the latter consequence is unavoidable, since it is a side effect of the discretization error of the finite-difference approximation in the case of spatially nonuniform curvature and/or nonuniform curvilinear grid. As explained in Sec. II A, this side effect can be minimized by choosing a sufficiently small grid size that prevents sharp curvature variations across one grid cell. If in addition the curvilinear grid is nonuniform, one should ensure sufficiently smooth grid size variations over neighboring grid cells.

C. The Peierls phase approximation

It is instructive to see how the matrix elements look in the limit of small curvature variations (smooth and slow transitions between different curvatures) and a weak magnetic field. For the matrix element $\boldsymbol{H}_n\,(m,m+1)$ the first condition allows us to write

$$e^{+\frac{1}{2}}_{n,m} \approx e^0_{n,m}, \quad e^{+\frac{1}{2}}_{n,m} \approx e^{+1}_{n,m}, \tag{22}$$

since the metric tensor varies very slowly over one unit cell in this limit. Further taking a weak magnetic field limit such that terms of the form $A_i\Delta_i$ are small, we obtain the following Peierls phase form:

$$\begin{aligned}\boldsymbol{H}_n(m,m+1) &\approx -f_2^{m-1}e^{+\frac{1}{2}}_{n,m-1}\left\{1 - \frac{ie}{\hbar}\frac{1}{2}\left[A_2(n,m-1)\Delta_2^{m-1} + A_2(n,m)\Delta_2^m\right]\right\}\\ &\approx -f_2^{m-1}e^{+\frac{1}{2}}_{n,m-1}\exp\left\{-\frac{ie}{\hbar}\frac{1}{2}\left[A_2(n,m-1)\Delta_2^{m-1} + A_2(n,m)\Delta_2^m\right]\right\}.\end{aligned} \tag{23}$$

Similarly,

$$\begin{aligned} \boldsymbol{H}_n(m,m-1) &\approx -f_2^{m-1} e_{n,m-1}^{-\frac{1}{2}} \exp\left\{\frac{ie}{\hbar}\frac{1}{2}\left[A_2(n,m-1)\Delta_2^{m-1} + A_2(n,m-2)\Delta_2^{m-2}\right]\right\}, \\ \boldsymbol{H}_{n,n\pm1}(m,m) &\approx -f_1^{n} d_{n,m-1}^{\pm\frac{1}{2}} \exp\left\{\mp\frac{ie}{\hbar}\frac{1}{2}\left[A_1(n,m-1)\Delta_1^{n} + A_1(n\pm1,m-1)\Delta_1^{n\pm1}\right]\right\}. \end{aligned} \tag{24}$$

Of course, there will be additional terms in Eq. (23) and the first of Eqs. (24) if we use the periodic boundary conditions in the u^2 direction, obtained by summing Eqs. (14) and (18) in a similar way. If we further neglect the remaining field-dependent term V_S from Eq. (6b), since it is second-order in magnetic vector components, we have represented the effect of the magnetic field in a curved nanoribbon through *the Peierls phase*, as is often done in planar nanostructures.[68,73]

In planar nanostructures subject to a perpendicular magnetic field, the Landau gauge with zero transverse component ($A_2 = 0$) is typically chosen to ensure plane-wave injection from the leads (more on this issue in the next section). Therefore, the phase in $\boldsymbol{H}_n(m,m\pm1)$ is typically zero in planar structures. In contrast, in curved nanostructures subject to a magnetic field, the curvature may make it impossible to eliminate A_2 through gauge transformations, so there may be nontrivial phase factors in $\boldsymbol{H}_n(m,m\pm1)$. We will discuss the issue of gauge transformations in the next section.

Let us estimate the magnitude of the magnetic field for which the Peierls phase approximation is justified. We can say $|\vec{A}| \approx |\vec{B}|D$, where D is the largest transverse dimension of the device. For the Peierls phase to hold we need

$$\frac{e}{\hbar}|\vec{A}|\Delta \ll 1,\ |\vec{B}| \ll \frac{\hbar}{e\Delta D} = \frac{6.6\times10^{-16}\mathrm{Tm}^2}{\Delta D}. \tag{25}$$

In a typical nanostructure, $\Delta \approx 1$ nm and $D \approx 100$ nm, so we have $|\vec{B}| \ll 6.6$ T. To estimate V_S, which depends on both the curvature and the magnetic field, we introduce R as the radius of curvature in our device and notice that $g_{ii} \sim R^2$. By again using $|\vec{A}| \approx |\vec{B}|D$ and Eq. (6b), we can easily show that $V_S \ll 1$ eV for $|\vec{B}| \ll \sqrt{m/|e|}/D$. We see that for V_S the condition is inversely proportional to D, which is reasonable because V_S is of the second order in $\vec{A}$ and, therefore, small for small device size. In GaAs and with $D \approx 100$ nm we have $V_S \ll 1$ eV for $|\vec{B}| \ll 6$ T, which is a similar condition as the one given by Eq. (25).

The Peierls phase approach is often used for simulating the effect of magnetic field in planar nanostructures.[68,73] Equation (19), modified such that matrix elements that contain the magnetic vector potential are given by Eqs. (23) and (24), along with setting $V_S = 0$, represent the generalization of that approach for curved nanostructures. Equations (23) and (24) reduce to the form used earlier for planar nanostructures in the limit of flat metric and a uniform grid, as do the other matrix elements in Eq. (19). Having in mind the approximations used to derive Eqs. (23) and (24) and to be able to neglect V_S, the Peierls phase approach for curved nanostructures has limited applicability for weak magnetic fields and small curvature variations. Since planar nanostructures are the limit of a flat metric (unit metric tensor, no curvature variations), the only condition for the Peierls phase approximation validity in them is a sufficiently weak magnetic field.

D. Handling the magnetic field: The local Landau gauge

In order to properly inject transverse modes and compute their velocities (the latter being critical for the calculation of the transmission matrix, as described in Appendix C 1), we have to include the leads in the transport calculation. A curved nanoribbon is placed between two leads that connect it to macroscopic reservoirs of charge. The leads act as the source/sink for the scattering states, whose plane-wave form in the leads allows us to calculate the conductance using the Landauer-Büttiker formalism.[67] So, we will include a necessary portion of the leads in the simulation region; in the case of planar leads, we will in general have to connect a planar rectangular grid of the leads to a curvilinear grid of a nanoribbon via a transition grid. The magnetic field will be present in the entire simulation region, including the leads. The basis that describes the lead/curved nanoribbon/lead system consists of scattering states, whose form in the injecting lead is a sum of the incident and reflected waves and in the outgoing lead a single transmitted wave.

In order to keep the scattering-state basis for the purposes of transport calculation in the presence of magnetic field, one has to use the Landau gauge in the planar leads, such that there is no transverse component of the magnetic vector potential in the leads and no explicit dependence on the longitudinal coordinate.[67] The Landau gauge ensures that the Hamiltonian eigenstates are plane waves along the longitudinal direction. In Fig. 2, we have an example of a lead injecting scattering states into a nanoribbon in toroidal geometry. The lead connects to the structure at the bottom left corner. The lead's Cartesian coordinate system, shown at the bottom left (z is the longitudinal coordinate in the lead, y is the transverse, and x is the normal coordinate) serves as the reference. We can write an arbitrary magnetic field, present in the whole structure, in terms of the lead's Cartesian coordinate system, $\vec{B} = (B_x, B_y, B_z)$, and define a Landau gauge for each component separately; namely we can define $\vec{A}^x = (0,0,B_x y)$, $\vec{A}^y = (0,0,-B_y x)$, and $\vec{A}^z = (-B_z y,0,0)$, so for an arbitrarily directed magnetic field $\vec{B}$, we can employ the superposition principle and write $\vec{A} = \vec{A}^x + \vec{A}^y + \vec{A}^z$. That is, the total magnetic vector potential will then be given by

$$\vec{A} = (-B_z y, 0, B_x y - B_y x). \tag{26}$$

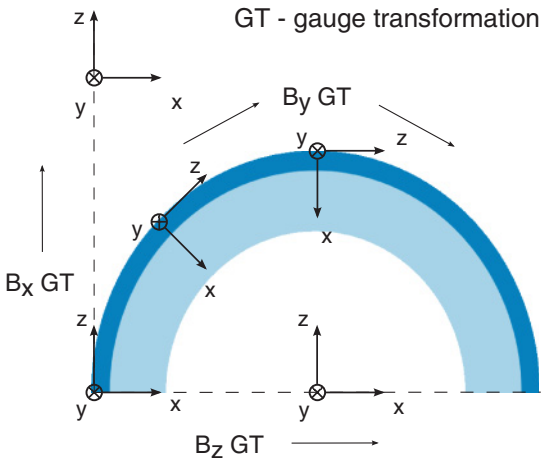

FIG. 2. (Color online) An example of a curved nanoribbon for calculating the magnetic vector potential: the nanoribbon (dark blue) on top of a half-torus (light blue), with the leads extending downward at both ends. The Cartesian coordinate system in the left lead (shown in the lower left corner) is taken as a reference system, according to which the magnetic field components B_x, B_y, and B_z are specified. Gauge transformations (GT), equivalent to coordinate system translations and rotations in the plane perpendicular to each component, are also shown.

With $\vec{A}$ in place for the injecting lead, we can calculate the injected scattering states by solving the eigenvalue problem of the transfer matrix between the first two slices that belong to the lead.[68] Explanation of one technical point is needed here. In order to obtain the correct number of forward- and backward-propagating states by numerically solving the eigenvalue problem in the lead, as in Appendix C, it is important to properly choose the reference level for $\vec{A}$. This can be done by centering the reference coordinate system to follow the midline that "cuts" the lead in half in the transverse direction: In other words, we can choose the $u^2 = 0$ grid line such that it extends into the lead and splits it in two halves symmetrically. On such a choice, the terms in $\vec{A}$ in Eq. (26) due to the different $\vec{B}$ components will always be either even or odd functions of the transverse position, which gives the correct number and distribution of forward- and backward-propagating states. We will refer to this $u^2 = 0$ line simply as the midline or the bisector. More details on the calculation and sorting of injected modes can be found in Appendix C.

Now, our nonplanar structure is placed between two leads, which could, in principle, be misaligned, and we need to be able to inject scattering states from both of them. It was shown (see Appendix E in Baranger and Stone[77]) that, in planar structures with misaligned leads, in order to have the Landau gauge and properly inject plane waves from each lead, one has to use suitable gauge transformations in order to properly account for the magnetic field in all leads. These gauge transformations ensure that the magnetic vector potential is calculated in the Landau gauge locally for each lead. The problem of including magnetic field in the presence of multiple misaligned leads is addressed in a similar way elsewhere.[78] In order to smoothly connect the magnetic vector potential in different leads, gauge transformations will be required in the device region as well. Since there is no unique analytical expression for gauge transformations for different geometries (like cylindrical or toroidal), we illustrate the approach with the aid of Fig. 2. We generalize the requirement to have a local Landau gauge in each lead to the requirement to have *a local Landau gauge in every slice of the lead/curved nanoribbon/lead system*.

The idea is the following: For a given magnetic field orientation, any coordinate system translation as well as coordinate system rotations in the plane perpendicular to the field can be shown to be equivalent to gauge transformations that make the gauge locally Landau.[77] In other words, if we define $\vec{A}$ associated with a given $\vec{B}$ in some coordinate system, then rotate and/or translate that system as specified above, after which we define $\vec{A}'$ in the transformed coordinate system in the same way as in the initial coordinate system (i.e., give it the same functional dependence on the new coordinates as we had in the old), then it can be shown that there exists a scalar function f such that (in the same set of coordinates, for instance, the old ones) $\vec{A}' = \vec{A} + \nabla f$. When employing the transfer matrix method, which uses slice-specific dynamical matrices as described in Sec. II B, the relevant matrices in each slice contain the magnetic vector potential according to the local Landau gauge (however, it is written in the curvilinear coordinates that parametrize the surface). Gauge-independent quantities, such as the electron density or conductance, are, of course, insensitive to these gauge transformations. In Appendix D 1, we show that the multitude of gauge transformations required to obtain the local Landau gauge slice by slice can be represented as a single gauge transformation.

In Fig. 2, we apply this approach to the magnetic vector potential components ($\vec{A}^x$, $\vec{A}^y$, or $\vec{A}^z$) generated by each magnetic field component (B_x, B_y, or B_z) independently, starting from Eq. (26) and having in mind the superposition principle. As already mentioned, we can always identify a midline through our device on which the reference coordinate system origin is situated in the reference (injecting) contact. The gauge transformations are then performed for each magnetic vector potential component ($\vec{A}^x$, $\vec{A}^y$, or $\vec{A}^z$) independently such that the coordinate system origin moves along the bisector from one lead to the other, while the local z axis is tangential to the projection of the bisector onto the plane normal to the respective magnetic field component. In the example of Fig. 2, nontrivial gauge transformations are needed only for the magnetic vector potential associated with the B_y field component, because it is the only field component requiring rotations; the projection of the bisector onto the plane normal to B_y is a semicircle (more details can be found in Appendix D 2). Projections of the bisector onto the planes normal to B_x and B_z are straight lines, and, thus, require only translations along the longitudinal axis (the z axis of the reference system for B_x and the x axis for B_z), while the values of the components of $\vec{A}$ in Eq. (26) related to these magnetic field components vary along the y axis, which is normal to the respective longitudinal axes and, therefore, neither directions nor values of these magnetic vector components are changed going from slice to slice.

III. EXAMPLES

We apply the method of Sec. II to calculate the electron density and conductance for various nanoribbons. To define curved nanoribbons of various shapes, we use a virtual substrate specified by a curvilinear coordinate system, like cylindrical, spherical, and torodial [in other words, we mimic placing the ribbon on top (or wrapping it around) a cylinder, sphere, or a torus] and then we apply a hardwall potential to define the ribbon edges. This method allows us to use relatively simple coordinate systems to work with complicated shapes. For each curvilinear coordinate system there are several quantities, related to the nonzero curvature, that have to be precalculated: the first fundamental form (or the metric tensor) g and the two principal curvatures, k_1 and k_2. Sufficient information for this task can be found in many textbooks and handbooks[74,79] and online mathematical resources.

A. Cylindrical geometry

The cylindrical geometry is relatively simple and very useful for modeling various curved nanoribbons that are being produced today.[4,7,23,80] We assume the ribbon will be placed on a cylinder of radius r, with (ϕ,x) being the natural surface coordinates and x being the direction of cylinder axis. By applying a hardwall potential in (ϕ,x) we can define the edges of the curved nanoribbon that is placed on top of or wrapped around the cylinder and proceed to calculate its conductance and electronic density by the previously described numerical technique. The leads are assumed cylindrical to avoid the need for transitional regions, which is a good approximation if the nanoribbon is narrow compared to the circumference of the cylinder. The leads extend away from both ends of the nanoribbon and along the cylinder axis, as depicted in Fig. 3(b).

In Figs. 3 and 4, we present calculation results for a cylindrical nanoribbon with helicity (wrapped around the cylinder) for two different magnetic field directions. The radius of the cylinder is $r = 40$ nm and its length is $4\pi r$, while the nanoribbon width corresponds to one-third of the circumference. The helix occupies one-half of the length. The Fermi level is at 8 meV, and the grid contains 500×250 points. The curved nanoribbon has no scattering centers; therefore, any difference between the actual normalized conductance and the number of injected propagating modes (formed in the injecting lead subject to the magnetic field), which can be seen in Figs. 3(a) and 4(a), is due to the curvature and helicity and their coupling with the magnetic field. For the direction of magnetic field as in Fig. 3(b), there is a very weak dependence of the Landau level energies in the injecting lead on the magnetic field, due to the fact that the field has a small flux through the narrow cylindrical lead, but the dependence is not strong enough to affect the number of injected propagating modes. (The flux would be zero if the leads were perfectly planar.) In Fig. 3(a), there are three modes injected throughout the magnetic field range, but even at $B = 0$ only two are transmitted; the reason for the reflection is the ribbon's helicity (we will discuss helicity in more detail later). From Fig. 3(a), we can see that, for higher magnetic fields, the transmission gradually decreases, until it is completely suppressed at around

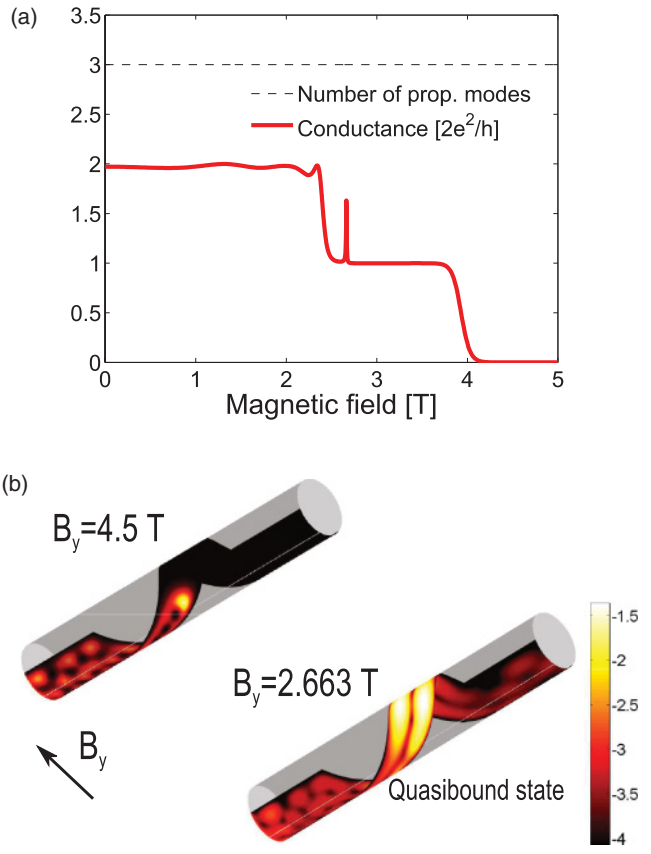

FIG. 3. (Color online) (a) Normalized conductance vs. magnetic field for a nanoribbon with helicity in cylindrical geometry. The leads are assumed cylindrical to avoid the need for transitional regions and, as a consequence, have the Landau levels energies affected by the magnetic field flux in the leads (Landau level quantization), albeit weakly. The lead on the left-hand side is the injecting lead. Magnetic field direction with respect to the structure is shown in (b) and would be parallel to the leads if they were exactly planar. Even at zero field, not all of the three injected modes propagate through, due to the ribbon helicity. (b) Electron density at the Fermi level shown for $B_y = 2.663$ T on the $\log_{10}$ scale, where there is resonant transmission, and for $B_y = 4.5$ T, where the normalized conductance is zero (transmission suppressed). A quasibound state [right panel of (b)] is associated with the resonant transmission feature from (a).

4 T. The suppression can also be observed in the plot of the electron density [Fig. 3(b)], where at 4.5 T the wave function is confined to the region close to the injecting lead. In contrast, at 2.663 T, a quasibound state is responsible for the resonant transmission, visible as a sharp peak in Fig. 3(a).

The variation in the Landau level energies in the leads with varying magnetic field is much more pronounced in Fig. 4, where the magnetic field is nearly perpendicular to the lead and produces maximal flux. Consequently, the number of injected propagating modes varies appreciably in the magnetic field range of interest. We use this example to illustrate the onset of discrepancies between a calculation based on the exact equation (19) and the Peierls phase approximation. The discrepancy between the curves calculated using the exact equation (19) and the Peierls phase approximation becomes apparent at fields higher than about 2.3 T, Fig. 4(a).

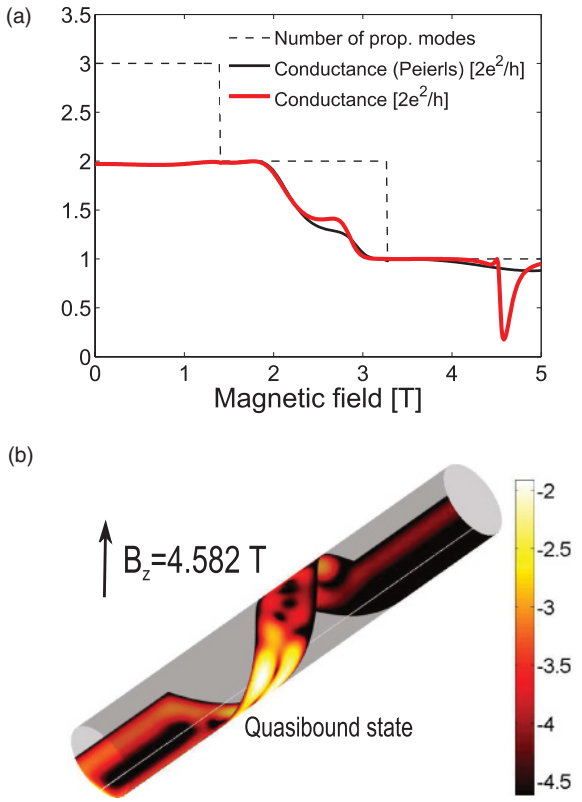

FIG. 4. (Color online) (a) Normalized conductance vs. magnetic field obtained with the exact equation (19) (thick solid red curve) and within the Peierls phase approach (thin solid black curve) for a nanoribbon with helicity in cylindrical geometry. The leads are assumed cylindrical to avoid the need for transitional regions. The lead on the left-hand side is the injecting lead. The magnetic field direction with respect to the structure is shown in (b) and would be normal to the leads if they were exactly flat. The number of injected propagating modes is shown with a thin dashed black curve and is influenced by the magnetic field flux in the leads (Landau level quantization). There is a discrepancy in the conductance between the exact and Peierls phase approaches starting at around 2.3 T. Resonant reflection is present at $B = 4.582$ T in the exact (thick red) curve. (b) Electron density at the Fermi level, represented through color on the $\log_{10}$ scale, corresponding to the resonant reflection at $B = 4.582$ T. A quasibound state is formed, primarily confined to the right-hand side of the helical part, looking from the left, injecting, lead.

The appearance of the resonant reflection (the sharp dip in transmission), often observed in 2D coherent electron systems of nonuniform width,[81–83] is present in the exact (thick red) curve at 4.582 T. In these nanostructures, although the nanoribbon has constant width (there are no cavities along the nanoribbon), the interplay between helicity and the magnetic field might lead to the formation of quasibound states responsible for resonant reflections. These reflections are very sensitive to the amplitude and direction of magnetic field. The interplay between the helicity and magnetic field is also responsible for the incomplete transmission from about 2 T to 3.3 T.

B. Toroidal geometry

Toroidal geometry is more complicated than the cylindrical one and enables us to demonstrate the technique on nanoribbons with spatially nonuniform curvature. We use a standard parametrization of a torus of radii R and r, where R is the radius of the large circle going through the middle of the torus and r is the radius of the small circle, whose center remains on the larger circle as its rotation around the large circle's axis maps the torus surface. The surface coordinates are the two angles, (θ,ϕ), where θ is related to r and ϕ to R. To avoid transitional regions, we adopt cylindrical leads here as well, because of their natural compatibility with a "straightened" torus. Having a curved nanoribbon that consists partially of a cylindrical shape and partially of a toroidal shape causes problems in constructing the tight-binding Hamiltonian, since the adopted longitudinal curvilinear coordinates have different units: length in the cylindrical part and angle in the toroidal part. To avoid this we can rescale the longitudinal coordinate in the torus to get the units of length there as well:

$$\theta \to \tilde{\theta} = c\theta, \quad \Delta_{1,\mathrm{tor}} \to \tilde{\Delta}_{1,\mathrm{tor}} = c\Delta_{1,\mathrm{tor}}, \tag{27}$$

where $\Delta_{1,\mathrm{tor}}$ is the longitudinal grid size in the toroidal part. The constant c has units of length and if we choose $c = \Delta_{1,\mathrm{cyl}}/\Delta_{1,\mathrm{tor}}$, we can, in addition to equating the units, obtain a uniform grid along the cylindrical lead-toroidal nanoribbon-cylindrical lead system. The corresponding change in the metric tensor is

$$\tilde{g}_{11} = \frac{\partial\vec{r}}{\partial\tilde{\theta}}\frac{\partial\vec{r}}{\partial\tilde{\theta}} = \frac{1}{c^2}\frac{\partial\vec{r}}{\partial\theta}\frac{\partial\vec{r}}{\partial\theta} = \frac{g_{11}}{c^2}. \tag{28}$$

Similarly, $\tilde{g}^{11} = c^2 g^{11}$ and $\tilde{g} = g/c^2$.

In Figs. 5–7 we present calculation results for several different nanoribbons in toroidal geometry, with and without a magnetic field. The radii of the torus are $R = 200$ nm and $r = 40$ nm. The Fermi level is at 8 meV, while the grid size is 575×230 for the toroidal part and 50×230 for each of cylindrical leads. The leads extend downward from the nanoribbon as shown in the electron density plots. This particular geometry, in combination with the magnetic field in the x direction [see the configuration in Fig. 5(b)] leads to one important point. Even though the leads can be geometrically equivalent, due to the combination of curvature and magnetic field, *the calculated transverse mode profiles in the leads might not be the same*. This fact requires a slight modification of the transfer matrix method by Usuki *et al.*[68] [see their Eq. (2.17)] to account for different mode-to-site conversion matrices in the incoming and outgoing leads. In Appendix C, we present the details of these necessary changes in case the two contacts cannot accommodate the same mode profile.

In Fig. 5, for the magnetic field along the x axis (the largest flux through the leads), we see that the actual conductance follows the number of propagating modes for most of the magnetic field magnitudes applied (there is no nanoribbon helicity) and then undergoes oscillating behavior when the magnetic field is sufficiently strong so there is only one propagating mode. This is a much more visible consequence of the resonant reflection, mentioned in connection to Fig. 4. In Fig. 5(b) electron density plots are shown for two characteristic points: zero conductance at $B_z = 4.456$ T (resonant reflection) and

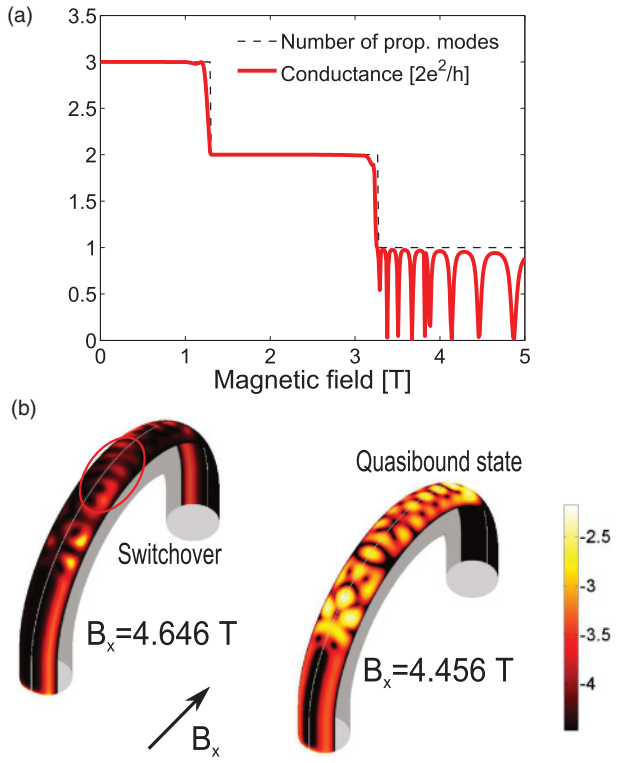

FIG. 5. (Color online) (a) Normalized conductance vs. magnetic field for a nanoribbon in toroidal geometry. The leads are assumed cylindrical to avoid the need for transitional regions. The number of propagating modes, given by the dashed line, is influenced by the magnetic field in the leads (Landau level quantization). There are strong resonant reflections at high magnetic fields, where there is only one injected mode. (b) Electron density at the Fermi level, represented through color, for unit conductance (complete transmission) at $B_x = 4.646$ T and zero conductance (resonant reflection) at $B_x = 4.456$ T. For complete transmission at $B_x = 4.646$ T, there is an edge channel formed that changes sides according to what can be expected from the classical Lorentz force. An extended quasibound state, responsible for the resonant reflection, is visible on the $\log_{10}$ scale in the central region of the nanoribbon at $B_x = 4.456$ T.

unit conductance (complete transmission) at $B_z = 4.646$ T. An extended quasibound state in the middle part of the nanoribbon is visible in the electron density plot in the $\log_{10}$ scale at $B_z = 4.456$ T, while for the case of complete transmission there is an edge state that changes sides according to what can be expected from the classical Lorentz force.

Figure 6 illustrates a situation where it is necessary to include gauge transformations, as explained in Sec. II D and Appendix D 2. Since the magnetic field is in the y direction (perpendicular to the plane of the torus and leads), the projection of the bisector (the middle longitudinal grid line of the nanoribbon) onto the plane normal to the magnetic field is a half-circle. In each slice perpendicular to the current flow, a local coordinate system (as depicted in Fig. 2) is rotated with respect to the reference system; each such rotation in the plane perpendicular to the magnetic field results in a gauge transformation. Therefore, we have a series of slice-dependent local Landau gauges as we move along the nanoribbon, which in this specific case means that $A_2 = 0$.

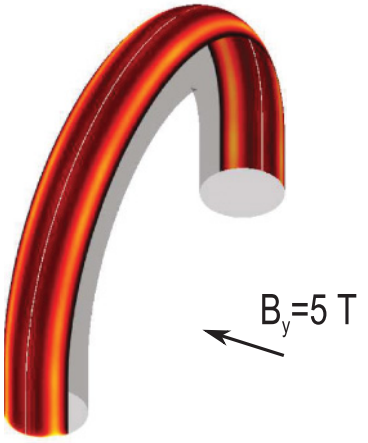

FIG. 6. (Color online) Sample electron density plot at the Fermi level for a toroidal nanoribbon subject to a magnetic field in the y direction. Electron density is represented through color (light denotes high and dark denotes low). This situation illustrates the use of the gauge transformations, as explained in Sec. II D and Appendix D 2, since the projection of the middle longitudinal grid line on the plane normal to the field is a half-circle, which requires the use of rotations in every slice of the toroidal part of the nanoribbon. The formed edge state reflects the symmetry of the problem and agrees qualitatively (the side at which it is formed) with the result obtained by applying the classical Lorentz force.

The edge state visible in the plot of electron density corresponds qualitatively (the side at which it is formed) to what can be expected from the classical Lorentz force and reflects well the symmetry of the problem. The details on how one performs the gauge transformations in this case in order to connect the local (slice-by-slice) Landau gauges are given in Appendix D 2.

In Fig. 7, we can see the results for a torodial nanoribbon, with and without helicity, in the absence of magnetic field. The normalized conductance for the nanoribbon without helicity agrees exactly with the number of injected propagating modes, meaning that there is complete transmission. Comparing the result of the conductance vs. Fermi level for the nanoribbons with and without helicity confirms that the observed difference between the normalized conductance and the number of propagating modes is due to helicity. As we also observed in Figs. 3 and 4, helicity plays a role similar to a quantum point contact in a flat wire (i.e., has the ability to quench propagation of certain modes). As shown earlier,[84] even without magnetic field one might expect resonant conductance features. The reason we do not see them here is because, due to the relatively large radius of the curvature of the nanoribbons considered here, the geometric potential is on the order of 0.1 meV, which is much smaller then the Fermi energy (8 meV). Another reason is that there are no sharp changes in curvature and, therefore, no sharp variations in the geometric vector potential, which can cause quantum interference effects.

IV. SUMMARY AND CONCLUDING REMARKS

We presented a theoretical and numerical technique for investigating the linear, ballistic transport properties of curved nanoribbons in a static, uniform, and arbitrarily directed

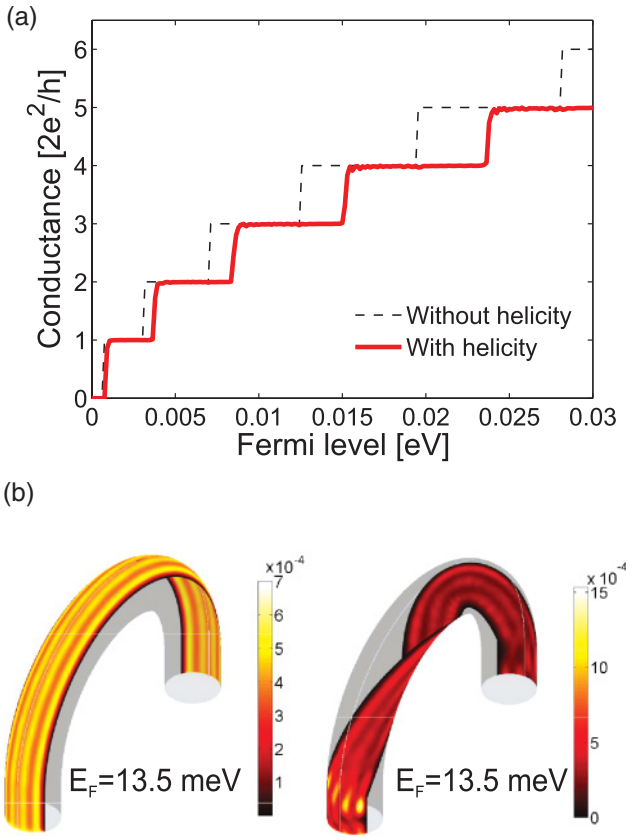

FIG. 7. (Color online) (a) Normalized conductance vs. Fermi level in the leads for a nanoribbon in toroidal geometry with and without helicity, in the absence of magnetic field. The leads are assumed cylindrical to avoid the need for transitional regions. The number of injected modes is changing due to the change in the Fermi energy. Comparison of the conductance for these two nanoribbons shows that helicity is the reason for the observed difference between the actual normalized conductance and the number of propagating modes. (b) Normalized electron density at the Fermi level, represented through color (white denotes high and black denotes low) for the nanoribbons with (right panel) and without helicity (left panel) when the Fermi level energy is equal to 13.5 meV.

magnetic field. Having started from the two-dimensional curvilinear Schrödinger equation with magnetic vector and electric scalar potentials included, after a rearrangement and rescaling of the Schrödinger equation we identified an effective potential, which is in general a complex quantity and depends on the magnetic field. The resulting equation was cast into a tight-binding form by using a second-order finite-difference scheme, which can be conveniently solved by a stabilized transfer matrix method. We analyzed the constraints on the Hermiticity of the discretized curvilinear Hamiltonian and proposed several suitable finite-difference schemes. While we adopted orthogonal coordinate systems throughout this paper, the framework is general enough that it can be extended to nonorthogonal coordinate systems if required.

Special attention was paid to the way in which the magnetic field should be included in the model. The requirement of working in the scattering-state basis, coupled with the structure's curvature, led us to a model for the inclusion of the magnetic field through *a local Landau gauge*. The use of the local Landau gauge is necessary to properly inject modes from the leads and avoid artificial numerical suppression of mode propagation, which can happen in finite-difference approaches to solving the Schrödinger equation in magnetic field, because an inadequate gauge in the effective complex potential *de facto* acts as a barrier to transmission. We have explained how slice-by-slice gauge transformations can be generated based on the structure's shape and the magnetic field direction.

Since the Peierls phase is often used to account for the magnetic field in planar nanostructures, we have also investigated the requirements for the validity of the Peierls phase approximation generalized to curved structures, where the magnetic field influence is captured through complex exponential terms. We find that there exists an upper limit on the magnetic field strength and curvature variations, connected to the structure's dimensions as well as the grid size, beyond which the Peierls phase approach is no longer valid.

We illustrated the method by numerically calculating the electron density at the Fermi level and conductance for several cylindrical and toroidal nanoribbons, with and without helicity, and subject to magnetic fields of different orientations. Interesting features that demonstrate the interplay between geometry and the magnetic field can be observed in these structures: For example, the prominent resonant reflection conductance features that occur due to a formation of bound states can be manipulated by curvature, helicity, and magnetic field.

ACKNOWLEDGMENT

The authors thank R. Joynt for helpful discussions. This work was supported by the NSF, Grant No. ECCS-0547415.

APPENDIX A: THE SURFACE DIVERGENCE OF THE MAGNETIC VECTOR POTENTIAL

By using the fact that $\nabla \cdot \vec{A} = 0$ for the Landau gauge in the Cartesian coordinate system and that the curvilinear coordinate system we are using is orthogonal, we derive a relationship between the surface curvilinear divergence $\nabla_S \cdot \vec{A}_S$ and the normal component A_3 and curvature properties, given by Eq. (5).

Since $\nabla \cdot \vec{A} = 0$ in the rectangular coordinate system, it will remain zero in any other coordinate system. So if we assume a general curvilinear coordinate system suitable for defining a curved surface in the limit where the thickness goes to zero,[59] we get

$$\nabla \cdot \vec{A} = \frac{1}{\sqrt{G}}\partial_i(\sqrt{G}G^{ij}A_j) = \frac{1}{\sqrt{G}}\partial_a(\sqrt{G}G^{ab}A_b) + \frac{1}{\sqrt{G}}\partial_3(\sqrt{G}A_3) = 0. \quad \text{(A1)}$$

Here, a and b are the surface curvilinear coordinates and

$$\boldsymbol{G} = \begin{bmatrix} G_{11} & G_{12} & 0 \\ G_{21} & G_{22} & 0 \\ 0 & 0 & 1 \end{bmatrix}, \quad \text{(A2)}$$

where G is the determinant of the matrix (A2) and G^{ij} are the contravariant components. If we evaluate Eq. (A1) at $u^3 = 0$, we get

$$\frac{1}{\sqrt{g}}\partial_a(\sqrt{g}g^{ab}A_b|_{u^3=0}) = -\frac{1}{\sqrt{G}}\partial_3(\sqrt{G}A_3)\Big|_{u^3=0}, \quad \text{(A3)}$$

since

$$G_{ab} = g_{ab} + \left[\tilde{\alpha}\boldsymbol{g} + (\tilde{\alpha}\boldsymbol{g})^T\right]_{ab}u^3 + \left(\tilde{\alpha}\boldsymbol{g}\tilde{\alpha}^T\right)_{ab}(u^3)^2 \quad \text{(A4)}$$

and $\tilde{\alpha}$ is a matrix with elements satisfying Weingarten equations[59]

$$\alpha_{11} = \frac{1}{g}(g_{12}h_{21} - g_{22}h_{11}), \quad \alpha_{12} = \frac{1}{g}(h_{11}g_{21} - h_{21}g_{11}),$$
$$\alpha_{21} = \frac{1}{g}(h_{22}g_{12} - h_{12}g_{22}), \quad \alpha_{22} = \frac{1}{g}(h_{21}g_{12} - h_{22}g_{11}). \quad \text{(A5)}$$

Using the fact that the coordinate system is orthogonal ($g_{12} = g_{21} = 0$) and that in our notation $\vec{A}_S = (A_1|_{u^3=0}, A_2|_{u^3=0}, 0)$, where $A_{1,2,3}$ are the covariant components of the magnetic vector potential, after some algebra we arrive at the final equation (5) from (A3).

APPENDIX B: HERMITICITY OF THE EXACT AND TIGHT-BINDING HAMILTONIANS

1. Exact Hamiltonian

Here, we will investigate the Hermiticity property of the exact Hamiltonian, given by Eq. (1). The first term on the left-hand side of Eq. (1) is the curvilinear Laplacian and it is well known that it is Hermitian. Therefore, we will not give the formal proof, but the method is similar to the one we will use for other terms. The fourth term on the left-hand side is real and does not contain any derivatives, so it is Hermitian, too. The terms that are not obviously Hermitian are the imaginary terms containing the magnetic vector potential (the second and third terms on the left-hand side). If we introduce $h = (ie\hbar/m)g^{ij}A_i\partial_j + iV_3$, we need to prove

$$\int \phi^*(h\psi)\,dS = \int (h\phi)^*\psi\,dS, \quad \text{(B1)}$$

where dS is an infinitesimal surface element on the curved surface S. It is known that the infinitesimal volume element can be expressed in a curvilinear coordinate system as[79] $dV = \sqrt{G}du^1du^2du^3$, where the three-dimensional metric tensor G_{ij} is defined in Appendix A. We can now write

$$(dV)_{u^3=0} = \sqrt{g}du^1du^2du^3 \quad \Rightarrow \quad dS = \sqrt{g}du^1du^2. \quad \text{(B2)}$$

The first term in h consists of a sum of four terms (two if the curvilinear coordinate system is orthogonal). For example, for $(i,j) = (1,1)$, we can use the integration by parts and the fact that the wave function vanishes at infinity:

$$\frac{ie\hbar}{m}\int du^2\int du^1\phi^*g^{11}A_1\sqrt{g}\partial_1\psi$$
$$= \left\{\begin{matrix} u=\phi^*g_{11}A_1\sqrt{g} \\ dv=\partial_1\psi du^1 \end{matrix}\right\} = \frac{ie\hbar}{m}\int du^2\Big[\psi\phi^*g^{11}A_1\sqrt{g}|_{u^1=-\infty}^{u^1=+\infty}$$
$$-\int\psi\partial_1(\phi^*g^{11}A_1\sqrt{g})du^1\Big]$$
$$= -\frac{ie\hbar}{m}\int\psi\partial_1(\phi^*g^{11}A_1\sqrt{g})du^1du^2$$
$$= -\frac{ie\hbar}{m}\Big[\int\psi g^{11}A_1\partial_1\phi^*dS$$
$$+\int\psi\phi^*\frac{1}{\sqrt{g}}\partial_1(\sqrt{g}g^{11}A_1)dS\Big]. \quad \text{(B3)}$$

Similar derivations can be carried out for the other three terms, so we have in total for the first term in h

$$\frac{ie\hbar}{m}\int\phi^*g^{ij}A_i\partial_j\psi dS$$
$$= -\frac{ie\hbar}{m}\Big[\int\psi g^{ij}A_i\partial_j\phi^*dS$$
$$+\int\psi\phi^*\frac{1}{\sqrt{g}}\partial_i(\sqrt{g}g^{ij}A_j)dS\Big]. \quad \text{(B4)}$$

The second term on the right-hand side in Eq. (B4) is the matrix element of $-2iV_3$. After the partial cancellation with iV_3 in h we then have

$$\int\phi^*(h\psi)\,dS = -\frac{ie\hbar}{2m}\int\psi\phi^*\frac{1}{\sqrt{g}}\partial_i(\sqrt{g}g^{ij}A_j)dS$$
$$-\frac{ie\hbar}{m}\int\psi g^{ij}A_i\partial_j\phi^*dS = \int(h\phi)^*\psi dS, \quad \text{(B5)}$$

which proves the Hermiticity of the exact Hamiltonian.

2. Tight-binding Hamiltonian

The tight-binding Hamiltonian derived by using finite-difference schemes does not have to be Hermitian, regardless of the fact the exact Hamiltonian is Hermitian. However, it is computationally advantageous to have Hermitian matrices when one wants to solve the eigenvalue problem. Here, we will show that the discretization schemes employed in Secs. II A and II B, along with some matrix transformations, allow for the definition of Hermitian matrices. To obtain the tight-binding Hamiltonian, we can rewrite Eq. (19) in the form of an eigenvalue problem. We have

$$\begin{bmatrix} \mathbf{H}_0 & \mathbf{H}_{0,1} & \mathbf{0} & \cdots & \mathbf{0} \\ \mathbf{H}_{1,0} & \mathbf{H}_1 & \mathbf{H}_{1,2} & \cdots & \mathbf{0} \\ \mathbf{0} & \mathbf{H}_{2,1} & \mathbf{H}_2 & \cdots & \mathbf{0} \\ \vdots & \vdots & \vdots & \vdots & \vdots \\ \mathbf{0} & \cdots & \mathbf{0} & \mathbf{H}_{N,N-1} & \mathbf{H}_N \end{bmatrix}\begin{bmatrix} \boldsymbol{\Psi}_0 \\ \boldsymbol{\Psi}_1 \\ \boldsymbol{\Psi}_2 \\ \vdots \\ \boldsymbol{\Psi}_N \end{bmatrix}$$
$$= E\begin{bmatrix} \mathbf{G}_0 & \mathbf{0} & \cdots & \cdots & \mathbf{0} \\ \mathbf{0} & \mathbf{G}_1 & \mathbf{0} & \cdots & \mathbf{0} \\ \mathbf{0} & \mathbf{0} & \mathbf{G}_2 & \cdots & \mathbf{0} \\ \vdots & \vdots & \vdots & \vdots & \vdots \\ \mathbf{0} & \cdots & \cdots & \mathbf{0} & \mathbf{G}_N \end{bmatrix}\begin{bmatrix} \boldsymbol{\Psi}_0 \\ \boldsymbol{\Psi}_1 \\ \boldsymbol{\Psi}_2 \\ \vdots \\ \boldsymbol{\Psi}_N \end{bmatrix} - \begin{bmatrix} \mathbf{A} \\ \mathbf{0} \\ \vdots \\ \mathbf{0} \\ \mathbf{B} \end{bmatrix}, \quad \text{(B6)}$$

where $\mathbf{A} = \mathbf{H}_{0,-1}\boldsymbol{\Psi}_{-1}$ and $\mathbf{B} = \mathbf{H}_{N,N+1}\boldsymbol{\Psi}_{N+1}$ are the open boundary conditions. If we extend all the matrices to include slices sufficiently far away from the curved region, we will

eventually be able to use the Dirichlet boundary conditions (analytically the wave function vanishes at infinity), so $\mathbf{A} = \mathbf{0}$ and $\mathbf{B} = \mathbf{0}$. We then can write the eigenvalue problem as

$$\mathbf{H}\Psi = E\mathbf{G}\Psi, \tag{B7}$$

where the matrix definitions follow from Eq. (B6) with $\mathbf{A} = \mathbf{0}$ and $\mathbf{B} = \mathbf{0}$.

As mentioned in Sec. (II A), one of the consequences of using the second-order discretization scheme is that the final tight-binding Hamiltonian matrix $\mathbf{G}^{-1}\mathbf{H}$ will not be Hermitian due to the existence of the curvilinear Laplacian. By rescaling the Schrödinger equation [Eq. (8)] we eventually arrived at a generalized eigenvalue problem given by Eq. (B7), where $\mathbf{H}$ is the rescaled tight-binding Hamiltonian matrix. Using a suitable matrix transformation we can obtain the eigenvalue problem in a standard form

$$\mathbf{H}\tilde{\mathbf{G}}^{-1}\tilde{\mathbf{G}}\Psi = E\tilde{\mathbf{G}}\tilde{\mathbf{G}}\Psi, \quad (\tilde{\mathbf{G}}^{-1}\mathbf{H}\tilde{\mathbf{G}}^{-1})\tilde{\mathbf{G}}\Psi = E\tilde{\mathbf{G}}\Psi, \tag{B8}$$

where the definition of $\tilde{\mathbf{G}}$ is obvious, since $\mathbf{G} = \tilde{\mathbf{G}}\tilde{\mathbf{G}}$ and $\mathbf{G}$ is diagonal. In this transformed eigenvalue problem, the Hamiltonian is given by $\tilde{\mathbf{G}}^{-1}\mathbf{H}\tilde{\mathbf{G}}^{-1}$ and the wave function by $\tilde{\mathbf{G}}\Psi$. Since the matrix $\tilde{\mathbf{G}}$ is diagonal, the condition for Hermiticity of this transformed Hamiltonian reduces to $\mathbf{H} = \mathbf{H}^{\dagger}$, where $\dagger$ represents the conjugate transpose. Furthermore, this condition reduces to

$$\left\{ \begin{array}{c} \mathbf{H}_n = \mathbf{H}_n^{\dagger} \\ \mathbf{H}_{n,n\pm1} = \mathbf{H}_{n\pm1,n}^{\dagger} \end{array} \right\} \Rightarrow \left\{ \begin{array}{c} \mathbf{L}_n = \mathbf{L}_n^{\dagger} \\ \mathbf{L}_{n,n\pm1} = \mathbf{L}_{n\pm1,n}^{\dagger} \\ \mathbf{P}_n = \mathbf{P}_n^{\dagger} \\ \mathbf{P}_{n,n\pm1} = \mathbf{P}_{n\pm1,n}^{\dagger} \end{array} \right\}, \tag{B9}$$

where we used definitions from Eq. (21).

If our curvilinear grid is uniform, such that $\Delta_1^n = \text{const} = \Delta_1$ and $\Delta_2^m = \text{const} = \Delta_2$, the conditions in Eq. (B9) are satisfied, as can be seen from Eqs. (12a)–(14) and Eqs. (17) and (18). Therefore, the eigenvalue problem in Eq. (B8) contains a Hermitian matrix. Since, in general, we prefer the possibility of using a nonuniform curvilinear grid, with Δ_1^n varying in the longitudinal direction and Δ_2^m in the transversal direction, the rescaled Hamiltonian matrix $\mathbf{H}$ will not be Hermitian. In that case we can introduce further matrix transformations,[85–87] defined by a diagonal block matrix $\mathbf{F}$, with diagonal matrices $\mathbf{F}_n$ on its main diagonal given by

$$\mathbf{F}_n(m,m) = \frac{2}{\sqrt{\left(\Delta_1^n + \Delta_1^{n-1}\right)\left(\Delta_2^{m-1} + \Delta_2^{m-2}\right)}}, \tag{B10}$$

where, as before, the index m on the left-hand side designates matrix elements with limits $m \in [1, M+1]$, while on the right-hand side all the quantities are defined on the grid having limits $[0, M]$ and, therefore, we use $m-1$ instead of m. We can now construct a Hermitian eigenvalue problem by the following matrix transformation in the second of Eqs. (B8):

$$(\mathbf{F}^{-1}\tilde{\mathbf{G}}^{-1}\mathbf{H}\mathbf{F}\mathbf{F}^{-1}\tilde{\mathbf{G}}^{-1})\tilde{\mathbf{G}}\Psi = E\mathbf{F}^{-1}\tilde{\mathbf{G}}\Psi,$$
$$(\tilde{\mathbf{G}}^{-1}\mathbf{F}^{-1}\mathbf{H}\mathbf{F}\tilde{\mathbf{G}}^{-1})\tilde{\mathbf{G}}\mathbf{F}^{-1}\Psi = E\tilde{\mathbf{G}}\mathbf{F}^{-1}\Psi,$$

which can be rewritten as

$$\overline{\mathbf{H}}\Phi = E\Phi, \tag{B11}$$

where $\overline{\mathbf{H}} = \tilde{\mathbf{G}}^{-1}\mathbf{F}^{-1}\mathbf{H}\mathbf{F}\tilde{\mathbf{G}}^{-1}$ is a Hermitian matrix and $\Phi = \tilde{\mathbf{G}}\mathbf{F}^{-1}\Psi$.

APPENDIX C: STABILIZED TRANSFER MATRIX SOLUTION TO EQ. (19)

To solve Eq. (19) for the transmission/reflection coefficients and electron density, we first rearrange it in the transfer matrix form:

$$\begin{bmatrix} \Psi_n \\ \Psi_{n+1} \end{bmatrix} = \mathbf{T}_n \begin{bmatrix} \Psi_{n-1} \\ \Psi_n \end{bmatrix}, \tag{C1}$$

where the transfer matrix $\mathbf{T}_n$ is given by

$$\mathbf{T}_n = \begin{bmatrix} 0 & \mathbf{1} \\ -\mathbf{H}_{n,n+1}^{-1}\mathbf{H}_{n,n-1} & \mathbf{H}_{n,n+1}^{-1}(E\cdot\mathbf{G}_n - \mathbf{H}_n) \end{bmatrix}. \tag{C2}$$

For our case of linear (small temperature and bias) and ballistic transport we solve this equation only for $E = E_F$, where E_F is the Fermi level energy. Writing equations of the form given by Eq. (C1) for every slice in our curved nanoribbon we can connect the two slices at the interface with the left lead to the two slices at the interface with the right lead

$$\begin{bmatrix} \Psi_N \\ \Psi_{N+1} \end{bmatrix} = \mathbf{T}_N \cdots \mathbf{T}_0 \begin{bmatrix} \Psi_{-1} \\ \Psi_0 \end{bmatrix}, \tag{C3}$$

where the domain bounded by slices 0 and N belongs to the curved nanoribbon and the rest belongs to the left (smaller than 0) and right (greater than N) leads.

We now express the wave functions on the left- and right-hand sides of Eq. (C3) in terms of the reflection and transmission coefficients multiplying forward- and backward-propagating eigenfunctions of the leads. In the Landau gauge, these eigenfunctions are proportional (up to the normalization constant) to the product of plane waves along the lead and transverse modes.[67] The decomposition of the wave functions in Eq. (C3) is possible because each Ψ_n ("slice wave function") is a superposition of forward and backward traveling waves, with amplitudes determined by specific injection conditions as well as any reflection and transmission that the wave undergoes. For the wave incident at the left lead (with unit amplitude) we can write

$$\begin{bmatrix} \Psi_{-1} \\ \Psi_0 \end{bmatrix} = \mathbf{T}_L \begin{bmatrix} \mathbf{1} \\ \mathbf{r} \end{bmatrix}, \quad \begin{bmatrix} \Psi_N \\ \Psi_{N+1} \end{bmatrix} = \mathbf{T}_R \begin{bmatrix} \mathbf{t} \\ \mathbf{0} \end{bmatrix}, \tag{C4}$$

where

$$\mathbf{T}_{L/R} = \begin{bmatrix} \Psi_{L/R}^{+} & \Psi_{L/R}^{-} \\ \Psi_{L/R}^{+}\boldsymbol{\lambda}_{L/R}^{+} & \Psi_{L/R}^{-}\boldsymbol{\lambda}_{L/R}^{-} \end{bmatrix}, \tag{C5}$$

with

$$\begin{aligned} \Psi_{L/R}^{\pm} &= \left[\boldsymbol{\psi}_{0,L/R}^{\pm}, \ldots, \boldsymbol{\psi}_{M,L/R}^{\pm}\right], \\ \boldsymbol{\lambda}_{L/R}^{\pm} &= \mathrm{diag}\left[\lambda_{0,L/R}^{\pm}, \ldots, \lambda_{M,L/R}^{\pm}\right], \end{aligned} \tag{C6}$$

where $\boldsymbol{\psi}_{l,L/R}^{\pm}$ is the eigenfunction of the l-th transverse mode at the (-1)-th (for L) and N-th (for R) slice, where $+$ stands for forward and $-$ for backward propagation, while $\lambda_{l,L/R}^{\pm}$ (similar notation as for eigenfunctions) is a phase factor that represents the difference in phase between eigenfunction values at two neighboring slices (eigenfunctions are plane waves along the lead). It should be noted that $\Psi_{L/R}^{\pm}$ is a matrix of dimension

$(M+1)\times(M+1)$, while $\mathbf{\Psi}_n$ is a column vector of dimension $(M+1)\times 1$.

We can construct the matrices $\mathbf{T}_{L/R}$ by using the transfer matrix form [Eq. (C1)] within the leads (planar geometry) and knowing that wave function values at two neighboring slices in the leads differ only by a phase factor. We obtain the following eigenvalue problems for the left and right leads

$$\begin{bmatrix} 0 & \mathbf{1} \\ -\mathbf{H}_{0,1}^{-1}\mathbf{H}_{0,-1} & \mathbf{H}_{0,1}^{-1}(E_F\cdot\mathbf{1}-\mathbf{H}_0)\end{bmatrix}\begin{bmatrix}\boldsymbol{\psi}_{l,L}^{\pm}\\ \lambda_{l,L}^{\pm}\boldsymbol{\psi}_{l,L}^{\pm}\end{bmatrix} = \lambda_{l,L}^{\pm}\begin{bmatrix}\boldsymbol{\psi}_{l,L}^{\pm}\\ \lambda_{l,L}^{\pm}\boldsymbol{\psi}_{l,L}^{\pm}\end{bmatrix}, \tag{C7}$$

$$\begin{bmatrix} 0 & \mathbf{1} \\ -\mathbf{H}_{N+1,N+2}^{-1}\mathbf{H}_{N+1,N} & \mathbf{H}_{N+1,N+2}^{-1}(E_F\cdot\mathbf{1}-\mathbf{H}_{N+1})\end{bmatrix} \times\begin{bmatrix}\boldsymbol{\psi}_{l,R}^{\pm}\\ \lambda_{l,R}^{\pm}\boldsymbol{\psi}_{l,R}^{\pm}\end{bmatrix} = \lambda_{l,R}^{\pm}\begin{bmatrix}\boldsymbol{\psi}_{l,R}^{\pm}\\ \lambda_{l,R}^{\pm}\boldsymbol{\psi}_{l,R}^{\pm}\end{bmatrix}. \tag{C8}$$

Here, for the purpose of keeping the same notation as in Eq. (C1), slices 0 and 1 appear, but it should be considered that they belong to the leads. In fact, since the leads are planar and uniform and the magnetic field is also uniform, we could have chosen any other combination of three consecutive slices that belong to the same lead in Eqs. (C7) and (C8). Matrices $\mathbf{H}_0$, $\mathbf{H}_{0,\pm1}$ and $\mathbf{H}_{N+1}$, $\mathbf{H}_{N+1,N+1\pm1}$ follow from the matrices in Eq. (21) in the zero-curvature limit and are given in earlier papers on coherent transport in planar nanostructures.[68,73] Finally, we obtain the following matrix equation to be solved

$$\begin{bmatrix}\mathbf{t}\\ \mathbf{0}\end{bmatrix} = \mathbf{T}_R^{-1}\mathbf{T}_N\cdots\mathbf{T}_0\mathbf{T}_L\begin{bmatrix}\mathbf{1}\\ \mathbf{r}\end{bmatrix}. \tag{C9}$$

Straightforward solution of Eq. (C9) is not stable numerically because of the existence of evanescent waves (exponentially growing or decaying), whose numerical value can become extremely small or large after only a few matrix multiplications. We employ a stabilized iterative technique due to Usuki *et al.*[68] with two minor modifications: in the wave function calculation and in allowing the left and right lead Hamiltonians to differ (either through different geometry or magnetic field flux). The fact that the lead Hamiltonians can differ is made explicit in the above equations. The stabilized iterative version of Eq. (C9) for the calculation of transmission coefficients in the column vector $\mathbf{t}$ is

$$\begin{bmatrix}\mathbf{C}_1^{(j+1)} & \mathbf{C}_2^{(j+1)}\\ \mathbf{0} & \mathbf{1}\end{bmatrix} = \mathbf{T}_j\begin{bmatrix}\mathbf{C}_1^{(j)} & \mathbf{C}_2^{(j)}\\ \mathbf{0} & \mathbf{1}\end{bmatrix}\mathbf{P}^{(j)}, \quad -1\leqslant j\leqslant N+1, \tag{C10}$$

with $\mathbf{T}_{-1}=\mathbf{T}_L$ and $\mathbf{T}_{N+1}=\mathbf{T}_R^{-1}$ and

$$\mathbf{P}^{(j)} = \begin{bmatrix}\mathbf{1} & \mathbf{0}\\ \mathbf{P}_1^{(j)} & \mathbf{P}_2^{(j)}\end{bmatrix}. \tag{C11}$$

By using the block matrix inversion to calculate $\mathbf{T}_R^{-1}$ and setting $\mathbf{T}_R^{12}=\mathbf{1}$, $\mathbf{T}_R^{22}=\mathbf{0}$, where the position of the block matrix in $\mathbf{T}_R$ is denoted by the superscript [their value is not important because they are multiplied by $\mathbf{0}$ in Eq. (C4)] we get

$$\mathbf{T}_{N+1} = \begin{bmatrix}\mathbf{0} & \left[\mathbf{\Psi}_R^{+}\boldsymbol{\lambda}_R^{+}\right]^{-1}\\ \mathbf{1} & -\mathbf{\Psi}_R^{+}\left[\mathbf{\Psi}_R^{+}\boldsymbol{\lambda}_R^{+}\right]^{-1}\end{bmatrix}. \tag{C12}$$

The form of $\mathbf{P}^{(j)}$ and its block matrices is determined from the condition that the form of the matrix on the left-hand side of Eq. (C10) is satisfied. We obtain

$$\mathbf{P}_1^{(j)} = -\mathbf{P}_2^{(j)}\mathbf{T}_j^{21}\mathbf{C}_1^{(j)}, \quad \mathbf{P}_2^{(j)} = \left[\mathbf{T}_j^{21}\mathbf{C}_2^{(j)}+\mathbf{T}_j^{22}\right]^{-1}, \tag{C13}$$

where different block matrices in $\mathbf{T}_j$ are specified with the row and column numbers in the superscript. Starting from the initial conditions $\mathbf{C}_1^{(0)}=\mathbf{1}$ and $\mathbf{C}_2^{(0)}=\mathbf{0}$ and solving Eq. (C10) iteratively we obtain the transmission coefficients from

$$\mathbf{t} = \mathbf{C}_1^{(N+2)}. \tag{C14}$$

In a similar way for the reflection coefficients we have

$$\left[\mathbf{D}_1^{(j+1)}\mathbf{D}_2^{(j+1)}\right] = \left[\mathbf{D}_1^{(j)}\mathbf{D}_2^{(j)}\right]\mathbf{P}^{(j)}, \quad \mathbf{r} = \mathbf{D}_1^{(N+2)}, \tag{C15}$$

with the initial conditions $\mathbf{D}_1^{(0)}=\mathbf{0}$ and $\mathbf{D}_2^{(0)}=\mathbf{1}$.

For the calculation of electron density we define a new operator $\mathbf{\Phi}^{(j)}$, using the already calculated operator $\mathbf{P}^{(j)}$,

$$\mathbf{\Phi}^{(j-1)} = \mathbf{P}_1^{(j-1)}+\mathbf{P}_2^{(j-1)}\mathbf{\Phi}^{(j)}, \quad N+1\geqslant j\geqslant 1, \tag{C16}$$

with the initial condition $\mathbf{\Phi}^{(N+1)}=\mathbf{P}_1^{(N+1)}$. Now the electron density originating from a single transverse mode l in the injecting lead will be

$$n_l(n,m) = \left|\mathbf{\Phi}^{(n)}(m,l)\right|^2, \quad n\in[0,N], \tag{C17}$$

where the indices (n,m) represent longitudinal and transverse grid positions, respectively.

1. Velocities of propagating states in the presence of magnetic field

With $\vec{A}$ in place as in Eq. (26), we can calculate the injected (evanescent and propagating) scattering states from each lead by solving the eigenvalue problem of the transfer matrix between the first two slices ($n=-1,0$) that belong to the leads [here we make use of the fact that the scattering states in the leads are plane waves in the longitudinal (transport) direction][68]

$$\exp(ik_1\Delta_1)\begin{bmatrix}\mathbf{\Psi}_{-1}\\ \mathbf{\Psi}_0\end{bmatrix} = \boldsymbol{T}_0\begin{bmatrix}\mathbf{\Psi}_{-1}\\ \mathbf{\Psi}_0\end{bmatrix}, \quad \boldsymbol{T}_0 = \begin{bmatrix}0 & \mathbf{1}\\ -\boldsymbol{H}_{0,1}^{-1}\boldsymbol{H}_{0,-1} & \boldsymbol{H}_{0,1}^{-1}(E\cdot\mathbf{1}-\boldsymbol{H}_0)\end{bmatrix}, \tag{C18}$$

where k_1 denotes the longitudinal component of the wave vector. Leads are assumed planar, so the $\boldsymbol{H}$ matrices satisfy the tight-binding 2D SE for a planar grid,[68] into which Eq. (19) reduces in the limit of zero curvature ($g_{ii}=g^{ii}=1$). Explanation of one technical point is needed here. In order to obtain the correct forward- and backward-propagating states from a numerical solution to Eq. (C18), it is important to properly choose the reference level for $\vec{A}$. This can be done by centering the reference coordinate system to follow the midline that "cuts" the lead in half in the transverse

direction: In other words, we can choose the $u^2 = 0$ grid line such that it extends into the lead and splits it in two halves symmetrically. On such a choice, the terms in $\vec{A}$ in Eq. (26), due to the different $\vec{B}$ components, will always be odd (linear in y) or even (independent of y) functions of the transverse position, which gives correct number and distribution of forward- and backward-propagating states.[73]

A correct evaluation of velocities is important since one of our goals is to calculate the transmission through a curved nanoribbon,

$$T_{ij} = |t_{ij}|^2 v^{(i)}/v^{(j)}, \tag{C19}$$

where i is the outgoing mode index, j is the incoming mode index, with v_i and v_j being the corresponding velocities, while t_{ij} is the matrix of transmission amplitudes, Eq. (C14).

It turns out that the relation $v^{(l)} = \hbar k_1^{(l)}/m^*$, where $k_1^{(l)}$ for a propagating mode of index l is calculated as explained above, does not hold in the presence of a magnetic field.[77,88] To calculate the appropriate relationship we can use a tight-binding Hamiltonian on a planar grid in a magnetic field. By working in the $|n,m\rangle$ basis (n denotes slice index and m denotes the transverse index in a slice)

$$\hat{x}|n,m\rangle = n\Delta_1|n,m\rangle, \quad |\psi\rangle = \sum_{n,m} \psi_{n,m}|n,m\rangle \tag{C20}$$

and defining the velocity operator in the x direction (which is assumed longitudinal in the leads) as usual,

$$\hat{v} = \frac{1}{i\hbar}[\hat{x}, \hat{H}], \tag{C21}$$

we can define the velocity at the slice n as

$$v_n^{(l)} = [\langle\psi|\hat{v}|\psi\rangle]_n^{(l)} = \frac{2t_1\Delta_1}{\hbar} \sum_m |\psi_{n,m}|^2 \times \left[\sin\left(k_1^{(l)}\Delta_1\right) - \frac{e}{\hbar}\cos\left(k_1^{(l)}\Delta_1\right) A_1(n,m)\Delta_1\right]. \tag{C22}$$

Here, $\hat{H}$ is the Hamiltonian with the matrix representation given by Eq. (B6) in flat metric and with a uniform grid assumed in the leads, so t_1 is the longitudinal hopping energy. We also make use of the fact that for a sufficiently small grid size one can employ the translational operator of the form $\psi_{n\pm1,m} = \psi_{n,m}\exp(\pm ik_1\Delta_1)$.[89] In the Peierls phase approximation (weak magnetic field so a small $\vec{A}$) Eq. (C22) equals

$$v_n^{(l)} \approx \frac{2t_1\Delta_1}{\hbar} \sum_m |\psi_{n,m}|^2 \sin\left\{\left[k_1^{(l)} - \frac{e}{\hbar}A_1(n,m)\right]\Delta_1\right\}. \tag{C23}$$

As A_1 depends only on the transverse coordinate [a consequence of the Landau gauge, see (26)], the only dependence of the current on the slice index n would occur through the term $|\psi_{n,m}|^2$. However, since a mode's transversal profile is constant inside a lead of constant width, and is modulated by a plane wave in the longitudinal direction, its square amplitude does not depend on n for any m and velocity (and current) per mode is conserved between slices in the lead. Therefore, it is sufficient to evaluate the mode velocity at $(n = -1)$ in Eqs. (C22) and (C23).

APPENDIX D: LOCAL LANDAU GAUGE

1. Local Landau gauge: Gauge transformations

The local Landau gauge transformation can be defined in a formal mathematical language. In analogy with a misaligned multiterminal structure,[77] here we can derive very similar equations with a slightly different interpretation: A local Landau gauge in every lead becomes a local Landau gauge in every slice, while the planar device region between the leads, used to smoothly connect local Landau gauges in the leads, becomes the curved regions between slices used to smoothly connect local Landau gauges in slices. The slice at the position of the reference coordinate system is numbered 0 (slice -1 belongs to the left lead), so we can write for the gauge transformation between slices 0 and n

$$\vec{A}_n(\vec{x}_0) = \vec{A}_0(\vec{x}_0) + \nabla f_n(\vec{x}_0), \tag{D1}$$

where $\vec{x}_0$ is a point in the reference coordinate system, which is positioned at the slice 0. It is straightforward to derive the function f_n for an arbitrary rotation[77] and a translation needed for the gauge transformation between the magnetic vector potential at the 0th slice, $\vec{A}_0$, and the magnetic vector potential at nth slice, $\vec{A}_n$. The gauge transformation then generated by f_n in Eq. (D1) allows us to express $\vec{A}_n$ in the same form as $\vec{A}_0$ but in a different coordinate system, translated and rotated with respect to the reference coordinate system in which $\vec{A}_0$ is calculated (see Fig. 2). For example, if $\vec{A}_0 = -By_0\hat{\vec{x}}_0$, then $\vec{A}_n = -By_n\hat{\vec{x}}_n$.

The gauge transformation given by f_n should be turned on only at the position of nth slice and turned off at the positions of all other slices, whereas in the rest of the domain (curved nanoribbon's surface), it should be a smooth function. This can be achieved by multiplying f_n by the following auxiliary function:

$$\xi_n = \begin{cases} 1, & \text{on slice } n \\ \text{smooth}, & \text{between slices } n-1 \text{ and } n+1 \\ 0, & \text{everywhere else}. \end{cases} \tag{D2}$$

Equation (D1) now becomes

$$\vec{A}_n = \vec{A}_0 + \nabla(\xi_n f_n) = \vec{A}_0 + \nabla\xi_n f_n + \xi_n \nabla f_n. \tag{D3}$$

At the slice n, $\nabla\xi_n = 0$ and $\xi_n = 1$ and we have a correct gauge transformation, given by Eq. (D1) evaluated at the slice n. In the domain bounded by slices 0 to $n-1$ and $n+1$ to N both the auxiliary function and its gradient are zero, so there is no gauge transformation of the form generated by f_n. In the domain bounded by slices $n-1$ to $n+1$ both the auxiliary function and its gradient are nonzero and we have some unavoidable gauge transformation, but we are not interested in its exact form since we work on the discrete grid only (space between discrete slices is not included in our calculation). To generate the total gauge transformation we calculate functions f_i and ξ_i for each slice i and sum them up

$$f = \sum_{i=1}^{N} \xi_i f_i. \tag{D4}$$

For a magnetic field of general direction we can write the total magnetic vector potential in the following form:

$$\vec{A}_0 = \vec{A}_0^x + \vec{A}_0^y + \vec{A}_0^z, \tag{D5}$$

where the magnetic vector potential components are each due to a magnetic field component denoted by the superscript. Therefore, for Eq. (26) we have that $\vec{A}_0^x = B_{x_0} y_0 \hat{\mathbf{z}}_0$, $\vec{A}_0^y = -B_{y_0} x_0 \hat{\mathbf{z}}_0$, and $\vec{A}_0^z = -B_{z_0} y_0 \hat{\mathbf{x}}_0$. Since the curl operator is linear we can use the principle of superposition and apply the necessary gauge transformations independently to these magnetic vector potential components. By applying the semi-graphical and formal mathematical methods explained above, we can decide which component needs a gauge transformation and calculate it.

In deriving Eq. (5) we used the fact that $\nabla \cdot \vec{A} = 0$ in the Landau gauge. If we use the separation into components explained in the previous paragraph, we see that the components of $\vec{A}$ not requiring gauge transformations will not alter the fact that $\nabla \cdot \vec{A} = 0$. However, in general, we might have a field component that requires a gauge transformation generated by the function in Eq. (D4). If we designate the field component requiring a gauge transformation by q we have

$$\begin{aligned} \vec{A}^q &= \vec{A}_0^q + \nabla f = \vec{A}_0^q + \sum_{i=0}^{N} \nabla (\xi_i f_i) \\ &= \vec{A}_0^q + \sum_{i=0}^{N} [f_i \nabla \xi_i + \xi_i \nabla f_i]. \end{aligned} \tag{D6}$$

Therefore,

$$\begin{aligned} \nabla \cdot \vec{A}^q &= \nabla \cdot \vec{A}_0^q + \sum_{i=0}^{N} [2\nabla f_i \cdot \nabla \xi_i + f_i \nabla^2 \xi_i + \xi_i \nabla^2 f_i] \\ &= \sum_{i=0}^{N} [2\nabla f_i \cdot \nabla \xi_i + f_i \nabla^2 \xi_i + \xi_i \nabla^2 f_i], \end{aligned} \tag{D7}$$

since $\nabla \cdot \vec{A}_0^q = 0$, $\vec{A}_0^q$ (as well as any other $\vec{A}_i^q$) being in the Landau gauge. This is clearly nonzero for arbitrary point on the surface of the curved nanoribbon, but since we work on a discrete grid let us evaluate Eq. (D7) at the points belonging to some slice n:

$$\begin{aligned} (\nabla \cdot \vec{A}^q)_n &= (\nabla^2 f_n)_n = (\nabla \cdot \nabla f_n)_n = \left[\nabla \cdot \left(\vec{A}_n^q - \vec{A}_0^q\right)\right]_n \\ &= \left(\nabla \cdot \vec{A}_n^q - \nabla \cdot \vec{A}_0^q\right)_n = 0, \end{aligned} \tag{D8}$$

where we used the properties of the function ξ_i and the fact that all $\vec{A}_i^q$'s are in the Landau gauge. So, at the points on the grid we still have zero divergence, meaning that we can still use Eq. (5) to calculate V_3 on the grid.

2. Gauge transformation for Fig. 6

From Eq. (26) we see that

$$\vec{A}_0 = (0, 0, -B_{y_0} x_0). \tag{D9}$$

From our discussion in Sec. II D we know that the slice 0 does not need a gauge transformation: We can directly use Eq. (D9) evaluated at the slice 0, because the longitudinal axis (the z_0 axis for the B_{y_0} component) is already tangential to the bisector at the point of its intersection with the slice 0, and the coordinate system is positioned at that point. When we transform the coordinates in Eq. (D9) to our toroidal coordinates (θ, ϕ, r) and evaluate the result at the position of the slice 0 ($\phi_0 = 0$) we get

$$\vec{A}_0\left(\vec{x}_0^{(0)}\right) = \hat{\boldsymbol{\phi}} B_{y_0} r\,(\cos\theta - 1), \tag{D10}$$

where $\vec{x}_0^{(0)}$ are points for which $\vec{x}_0 \in \{\text{slice } 0\}$.

Angle ϕ is measured from the slice 0, which is at the interface with the left lead in Fig. 2, while angle θ is measured from the bisector toward the negative y_0 axis (where the y_0 axis belongs to the reference coordinate system in Fig. 2). If the Cartesian coordinate system is like the reference coordinate system in Fig. 2, but positioned in the center of the torus (from where R is measured), then the formulas relating the Cartesian coordinates of the torus surface (x, y, z) to the curvilinear coordinates (θ, ϕ) are given by

$$\begin{aligned} x = -(R + r\cos\theta)\cos\phi, \quad y = -r\sin\theta, \\ z = (R + r\cos\theta)\sin\phi, \end{aligned} \tag{D11}$$

where ϕ is measured from the negative x axis and θ in the clockwise direction looking along the current flow (from left to right in Fig. 2).

The transformation to the toroidal coordinates can be done by using Eq. (D11) and the following relations:

$$x_0 = x + R + r, \quad y_0 = y, \quad z_0 = z, \tag{D12}$$

$$\begin{aligned} \hat{\mathbf{x}}_0 &= \hat{\boldsymbol{\phi}}\sin\phi - \hat{\mathbf{r}}\cos\theta\cos\phi + \hat{\boldsymbol{\theta}}\sin\theta\cos\phi, \\ \hat{\mathbf{y}}_0 &= -\hat{\boldsymbol{\theta}}\cos\theta - \hat{\mathbf{r}}\sin\theta, \\ \hat{\mathbf{z}}_0 &= \hat{\boldsymbol{\phi}}\cos\phi + \hat{\mathbf{r}}\cos\theta\sin\phi - \hat{\boldsymbol{\theta}}\sin\theta\sin\phi. \end{aligned} \tag{D13}$$

Since we know that after the gauge transformation the form of $\vec{A}$ is the same, but expressed in a new coordinate system, which is translated and rotated according to the slice position (see Fig. 2 for the B_y component), we conclude that

$$\vec{A}_i\left(\vec{x}_i^{(i)}\right) = \hat{\boldsymbol{\phi}} B_{y_0} r\,(\cos\theta - 1), \quad 0 \leqslant i \leqslant N. \tag{D14}$$

Equation (D14) can be derived in a formal way by using Eq. (D1). If we assume that for some slice n the coordinate system (as shown in Fig. 2) is rotated by the angle α_n (clockwise here) and translated by the lengths a along the x_0 axis and b along the z_0 axis we obtain for f_n

$$\begin{aligned} f_n(\vec{x}_0) = B_{y_0}\Big[&(x_0 z_0 - b x_0)\sin^2\alpha_n + a z_0 \cos^2\alpha_n \\ &+ \frac{1}{2}\left(\frac{1}{2}z_0^2 - \frac{1}{2}x_0^2 - b z_0 + a x_0\right)\sin 2\alpha_n \Big]. \end{aligned} \tag{D15}$$

Now, since $\vec{A}_0 = -B_{y_0} x_0 \hat{\mathbf{z}}_0$, by using Eq. (D1) we obtain

$$\begin{aligned} \vec{A}_n(\vec{x}_0) = -B_{y_0}\Big\{ &\hat{\mathbf{z}}_0\left[(x_0 - a)\cos^2\alpha_n - \tfrac{1}{2}(z_0 - b)\sin 2\alpha_n\right] \\ &+ \hat{\mathbf{x}}_0\left[\tfrac{1}{2}(x_0 - a)\sin 2\alpha_n - (z_0 - b)\sin^2\alpha_n\right]\Big\}. \end{aligned} \tag{D16}$$

Using the transformations between coordinates (x_0, y_0, z_0) and (x_n, y_n, z_n)

$$\begin{aligned} x_0 &= a + z_n \sin\alpha_n + x_n \cos\alpha_n, \\ z_0 &= b + z_n \cos\alpha_n - x_n \sin\alpha_n, \end{aligned} \tag{D17}$$

$$\hat{\mathbf{x}}_0 = \hat{\mathbf{z}}_n \sin\alpha_n + \hat{\mathbf{x}}_n \cos\alpha_n,$$
$$\hat{\mathbf{z}}_0 = \hat{\mathbf{z}}_n \cos\alpha_n - \hat{\mathbf{x}}_n \sin\alpha_n, \qquad \text{(D18)}$$

it can be shown that, from Eq. (D16), $\vec{A}_n = -B_{y_0} x_n \hat{\mathbf{z}}_n$. On the other hand, by using the transformations between coordinates (x_0, y_0, z_0) and (θ, ϕ, r) given by Eqs. (D11) and (D12), along with the transformations between unit vectors in Eq. (D13), we obtain

$$\vec{A}_i\left(\vec{x}_0^{(i)}\right) = \hat{\boldsymbol{\phi}} B_{y_0} r\,(\cos\theta - 1)\,, \quad 0 \leqslant i \leqslant N, \qquad \text{(D19)}$$

where we used the facts that $\alpha_n = \phi_n$, $\sin\phi_n = b/(R+r)$, and $\cos\phi_n = (R + r - a)/(R + r)$. Equation (D19) is the same as Eq. (D14), previously obtained in an easier way, with the formal distinction in the argument of $\vec{A}_i$: the transformation to the toroidal coordinates in Eq. (D14) is done from the rotated and translated coordinate system (x_i, y_i, z_i), since we know $\vec{A}_i\,(\vec{x}_i)$ and $\vec{A}_0\,(\vec{x}_0)$ have the same form, while in Eq. (D19) it is from the reference coordinate system by formally deriving the gauge transformation according to Eq. (D1).

*novakovic@wisc.edu
†knezevic@engr.wisc.edu

[1] O. G. Schmidt and K. Eberl, Nature **410**, 168 (2001).
[2] A. J. Baca, J. H. Ahn, Y. G. Sun, M. A. Meitl, E. Menard, H. S. Kim, W. M. Choi, D. H. Kim, Y. Huang, and J. A. Rogers, Angew. Chem. Int. Ed. **47**, 5524 (2008).
[3] N. Shaji, H. Qin, R. H. Blick, L. J. Klein, C. Deneke, and O. G. Schmidt, Appl. Phys. Lett. **90**, 042101 (2007).
[4] F. Cavallo, R. Songmuang, and O. G. Schmidt, Appl. Phys. Lett. **93**, 143113 (2008).
[5] S. A. Scott and M. G. Lagally, J. Phys. D: Appl. Phys. **40**, R75 (2007).
[6] X. Li, J. Phys. D: Appl. Phys. **41**, 193001 (2008).
[7] V. Y. Prinz, V. A. Seleznev, A. K. Gutakovsky, A. V. Chehovskiy, V. V. Preobrazhenskii, M. A. Putyato, and T. A. Gavrilova, Physica E **6**, 828 (2000).
[8] S. V. Golod, V. Y. Prinz, V. I. Mashanov, and A. K. Gutakovsky, Semicond. Sci. Technol. **16**, 181 (2001).
[9] M. H. Huang, C. Boone, M. Roberts, D. E. Savage, M. G. Lagally, N. Shaji, H. Qin, R. Blick, J. A. Nairn, and F. Liu, Adv. Mater. **17**, 2860 (2005).
[10] O. G. Schmidt, C. D. Y. M. Manz, and C. Muller, Physica E **13**, 969 (2002).
[11] A. Lorke, S. Bohm, and W. Wegscheider, Superlattices Microstruct. **33**, 347 (2003).
[12] A. L. Ivanovskii, Russ. Chem. Rev. **71**, 175 (2002).
[13] J. Goldberger, R. R. He, Y. F. Zhang, S. W. Lee, H. Q. Yan, H. J. Choi, and P. D. Yang, Nature **422**, 599 (2003).
[14] A. K. Roy, S. Knohl, and W. A. Goedel, J. Mater. Sci. **46**, 4812 (2011).
[15] H. W. Kim, H. G. Na, and J. C. Yang, Chem. Eng. J. **170**, 326 (2011).
[16] H. M. Fan, J. B. Yi, Y. Yang, K. W. Kho, H. R. Tan, Z. X. Shen, J. Ding, X. W. Sun, M. C. Olivo, and Y. P. Feng, ACS NANO **3**, 2798 (2009).
[17] H. Yuan, Z. Ma, M. M. Roberts, D. E. Savage, and M. G. Lagally, J. Appl. Phys. **100**, 013708 (2006).
[18] H. Yuan, G. K. Celler, and Z. Ma, J. Appl. Phys. **102**, 034501 (2007).
[19] D. Kim, J. Ahn, W. M. Choi, H. Kim, T. Kim, J. Song, Y. Y. Huang, Z. Liu, C. Lu, and J. A. Rogers, Science **320**, 507 (2008).
[20] H. C. Ko *et al.*, Nature **454**, 748 (2008).
[21] E. Menard, R. G. Nuzzo, and J. A. Rogers, Appl. Phys. Lett. **86**, 093507 (2005).
[22] J.-U. Park *et al.*, Nat. Mater. **6**, 782 (2007).
[23] Y. Mei, G. S. Huang, A. A. Solovev, E. B. Urena, I. Moench, F. Ding, T. Reindl, R. K. Y. Fu, P. K. Chu, and O. G. Schmidt, Adv. Mater. **20**, 4085 (2008).
[24] T. Kipp, H. Welsch, C. Strelow, C. Heyn, and D. Heitmann, Phys. Rev. Lett. **96**, 077403 (2006).
[25] S. Mendach, R. Songmuang, S. Kiravittaya, A. Rastelli, M. Benyoucef, and O. G. Schmidt, Appl. Phys. Lett. **88**, 111120 (2006).
[26] S. Vicknesh, F. Li, and Z. Mi, Appl. Phys. Lett. **94**, 081101 (2009).
[27] G. S. Huang, S. Kiravittaya, V. A. B. Quinones, F. Ding, M. Benyoucef, A. Rastelli, Y. F. Mei, and O. G. Schmidt, Appl. Phys. Lett. **94**, 141901 (2009).
[28] M. Hosoda and T. Shigaki, Appl. Phys. Lett. **90**, 181107 (2007).
[29] F. Li, S. Vicknesh, and Z. Mi, Electron Lett. **45**, 645 (2009).
[30] Y. J. Xing, Z. H. Xi, Z. Q. Xue, X. D. Zhang, J. H. Song, R. M. Wang, J. Xu, Y. Song, S. L. Zhang, and D. P. Yu, Appl. Phys. Lett. **83**, 1689 (2003).
[31] I. S. Chun, K. Bassett, A. Challa, and X. L. Li, Appl. Phys. Lett. **96**, 251106 (2010).
[32] F. Li, Z. T. Mi, and S. Vicknesh, Opt. Lett. **34**, 2915 (2009).
[33] F. Li and Z. T. Mi, Opt. Express **17**, 19933 (2009).
[34] S. Schwaiger, M. Broll, A. Krohn, A. Stemmann, C. Heyn, Y. Stark, D. Stickler, D. Heitmann, and S. Mendach, Phys. Rev. Lett. **102**, 163903 (2009).
[35] D. V. Bulaev, V. A. Geyler, and V. A. Margulis, Phys. Rev. B **69**, 195313 (2004).
[36] C. Deneke, J. Schumann, R. Engelhard, J. Thomas, C. Muller, M. S. Khatri, A. Malachias, M. Weisser, T. H. Metzger, and O. G. Schmidt, Nanotechnology **20**, 045703 (2009).
[37] C. Muller, M. S. Khatri, C. Deneke, S. Fahler, Y. F. Mei, E. B. Urena, and O. G. Schmidt, Appl. Phys. Lett. **94**, 102510 (2009).
[38] T. R. Ger, C. C. Huang, H. T. Huang, and Z. H. Wei, J. Appl. Phys. **109**, 07E534 (2011).
[39] L. I. Magarill, D. A. Romanov, and A. V. Chaplik, J. Exp. Theor. Phys. **86**, 771 (1998).
[40] L. I. Magarill and A. V. Chaplik, J. Exp. Theor. Phys. **88**, 815 (1999).
[41] S. Mendach, J. Podbielski, J. Topp, W. Hansen, and D. Heitmann, Appl. Phys. Lett. **93**, 262501 (2008).
[42] F. Balhorn, S. Mansfeld, A. Krohn, J. Topp, W. Hansen, D. Heitmann, and S. Mendach, Phys. Rev. Lett. **104**, 037205 (2010).
[43] S. Ono and H. Shima, Phys. Rev. B **79**, 235407 (2009).
[44] S. Ono and H. Shima, Physica E **42**, 1224 (2010).
[45] H. Taira and H. Shima, Surf. Sci. **601**, 5270 (2007).

[46]G. Ferrari, A. Bertoni, G. Goldoni, and E. Molinari, Phys. Rev. B **78**, 115326 (2008).
[47]V. Atanasov, R. Dandoloff, and A. Saxena, Phys. Rev. B **79**, 033404 (2009).
[48]C. Ortix and J. van den Brink, Phys. Rev. B **81**, 165419 (2010).
[49]G. D. Valle and S. Longhi, J. Phys. B **43**, 051002 (2010).
[50]C. L. Foden, M. L. Leadbeater, and M. Pepper, Phys. Rev. B **52**, R8646 (1995).
[51]V. A. Margulis and M. A. Pyataev, Phys. Rev. B **72**, 075312 (2005).
[52]G. J. Meyer, N. L. Dias, R. H. Blick, and I. Knezevic, IEEE Trans. Nanotechnol. **6**, 446 (2007).
[53]G. Papp and F. M. Peeters, Solid State Commun. **149**, 778 (2009).
[54]M. L. Leadbeater, C. L. Foden, J. H. Burroughes, M. Pepper, T. M. Burke, L. L. Wang, M. P. Grimshaw, and D. A. Ritchie, Phys. Rev. B **52**, R8629 (1995).
[55]Y. Meir and N. S. Wingreen, Physica E **23**, 274 (2004).
[56]A. V. Chaplik and R. H. Blick, New J. Phys. **6**, 33 (2004).
[57]A. B. Vorob'ev, K. J. Friedland, H. Kostial, R. Hey, U. Jahn, E. Wiebicke, J. S. Yukecheva, and V. Y. Prinz, Phys. Rev. B **75**, 205309 (2007).
[58]K. J. Friedland, R. Hey, H. Kostial, A. Riedel, and K. H. Ploog, Phys. Rev. B **75**, 045347 (2007).
[59]R. C. T. da Costa, Phys. Rev. A **23**, 1982 (1981).
[60]M. Encinosa, Phys. Rev. A **73**, 012102 (2006).
[61]H. Jensen and H. Koppe, Ann. Phys. **63**, 586 (1971).
[62]M. Ikegami, Y. Nagaoka, S. Takagi, and T. Tanzawa, Prog. Theor. Phys. **88**, 229 (1992).
[63]G. Ferrari and G. Cuoghi, Phys. Rev. Lett. **100**, 230403 (2008).
[64]R. Landauer, IBM J. Res. Dev. **1**, 233 (1957).
[65]M. Büttiker, Phys. Rev. Lett. **57**, 1761 (1986).
[66]R. Landauer, Z. Phys. B **68**, 217 (1987).
[67]S. Datta, *Electronic Transport in Mesoscopic Systems* (Cambridge University Press, Cambridge, UK, 1995).
[68]T. Usuki, M. Saito, M. Takatsu, R. A. Kiehl, and N. Yokoyama, Phys. Rev. B **52**, 8244 (1995).
[69]S. Brand and D. T. Hughes, Semicond. Sci. Technol. **2**, 607 (1987).
[70]C. Mailhiot and D. L. Smith, Phys. Rev. B **33**, 8360 (1986).
[71]H. Tamura and T. Ando, Phys. Rev. B **44**, 1792 (1991).
[72] David Yuk Kei Ko and J. C. Inkson, Phys. Rev. B **38**, 9945 (1988).
[73]T. Ando, Phys. Rev. B **44**, 8017 (1991).
[74]G. A. Korn and T. M. Korn, *Mathematical Handbook for Scientists and Engineers: Definitions, Theorems, and Formulas for Reference and Review* (McGraw-Hill, New York, 1968).
[75]N. A. Modine, G. Zumbach, and E. Kaxiras, Phys. Rev. B **55**, 10289 (1997).
[76]F. Gygi and G. Galli, Phys. Rev. B **52**, R2229 (1995).
[77]H. U. Baranger and A. D. Stone, Phys. Rev. B **40**, 8169 (1989).
[78]D. Guan, U. Ravaioli, R. W. Giannetta, M. Hannan, I. Adesida, and M. R. Melloch, Phys. Rev. B **67**, 205328 (2003).
[79]K. F. Riley, M. P. Hobson, and S. J. Bence, *Mathematical Methods for Physics and Engineering* (Cambridge University Press, Cambridge, UK, 1997), p. 722.
[80]V. Y. Prinz and S. V. Golod, J. Appl. Mech. Tech. Phys. **47**, 867 (2006).
[81]W. Porod, Z. Shao, and C. S. Lent, Appl. Phys. Lett. **61**, 1350 (1992).
[82]H. Wu and D. W. L. Sprung, Phys. Rev. B **47**, 1500 (1993).
[83]R. Akis, P. Vasilopoulos, and P. Debray, Phys. Rev. B **52**, 2805 (1995).
[84]A. Marchi, S. Reggiani, M. Rudan, and A. Bertoni, Phys. Rev. B **72**, 035403 (2005).
[85]M. Luisier, A. Schenk, and W. Fichtner, J. Appl. Phys. **100**, 043713 (2006).
[86]M. Luisier and A. Schenk, IEEE Trans. Electron Devices **55**, 1494 (2008).
[87]I.-H. Tan, G. L. Snider, L. D. Chang, and E. L. Hu, J. Appl. Phys. **68**, 4071 (1990).
[88]R. Akis, R. Barnes, and G. Kirczenow, Can. J. Phys. **73**, 147 (1995).
[89]D. K. Ferry, *Quantum Mechanics: An Introduction for Device Physicists and Electrical Engineers* (IOP, Bristol, UK, 2001), p. 192.